PHYSICAL REVIEW B **82**, 035445 (2010)

Orbital order in bilayer graphene at filling factor $\nu=-1$

R. Côté,[1] Jules Lambert,[1] Yafis Barlas,[2] and A. H. MacDonald[3]
[1]*Département de Physique, Université de Sherbrooke, Sherbrooke, Québec, Canada J1K 2R1*
[2]*National High Magnetic Field Laboratory and Department of Physics, The Florida State University, Tallahassee, Florida 32306, USA*
[3]*Department of Physics, The University of Texas at Austin, Austin, Texas 78712, USA*
(Received 29 March 2010; revised manuscript received 14 June 2010; published 30 July 2010)

In a graphene bilayer with Bernal stacking, both $n=0$ and $n=1$ orbital Landau levels have zero kinetic energy. An electronic state in the $N=0$ Landau level consequently has three quantum numbers in addition to its guiding center label: its spin, its valley index K or K', and an orbital quantum number $n=0,1$. The two-dimensional electron gas (2DEG) in the bilayer supports a wide variety of broken-symmetry states in which the pseudospins associated with these three quantum numbers order in a manner that is dependent on both filling factor ν and the electric potential difference between the layers. In this paper, we study the case of $\nu=-1$ in an external field strong enough to freeze electronic spins. We show that an electric potential difference between layers drives a series of transitions, starting from an interlayer-coherent state (ICS) at small potential and leading to an orbitally coherent state (OCS) that is polarized in a single layer. Orbital pseudospins carry electric dipoles with orientations that are ordered in the OCS and have Dzyaloshinskii-Moriya interactions that can lead to spiral instabilities. We show that the microwave absorption spectra of ICSs and OCSs are sharply distinct.

DOI: 10.1103/PhysRevB.82.035445 PACS number(s): 73.21.−b, 73.22.Gk, 78.70.Gq

I. INTRODUCTION

Semiconductor double-quantum-well systems in a quantizing magnetic field develop spontaneous interlayer coherence when the wells are brought into close proximity.[1] Spontaneous coherence leads to a variety of fascinating transport effects including counterflow superfluidity and anomalous interlayer tunneling, and to unusual charged excitations such as merons. A convenient way to describe these ground states is to use a pseudospin language in which the *layer* degree-of-freedom is mapped to a $S=1/2$ pseudospin. In this language, the ground state of a bilayer at total filling factor $\nu=1$ is an easy-plane pseudospin ferromagnet. At higher filling factors, still more exotic states occur, for example states in which the layer pseudospin orientation varies in space and a charge-density-wave is formed.[2]

Interest has recently been growing in the strong-magnetic-field ordered states of graphene bilayers. Single layer graphene[3] is a two-dimensional honeycomb lattice network of carbon atoms. Bilayer graphene[4–6] consists of two graphene layers separated by a fraction of a nanometer. In the normal Bernal stacking structure, one of the two honeycomb sublattice sites in each layer has a near neighbor in the other layer, and one does not. This arrangement produces[4,5] a set of Landau levels with energies $E_N=\pm\hbar\omega_c^*\sqrt{|N|(|N|+1)}$ where ω_c^* is the effective cyclotron frequency and $N=0,\pm1,\pm2,\ldots$. All Landau levels except $N=0$ are fourfold degenerate; electronic states are specified by N, valley index (K or K') and spin index, in addition to the usual label used to specify guiding center states within a Landau level.

The $N=0$ Landau level has an additional two-valued quantum degree-of-freedom because states with both $n=0$ and $n=1$ Landau-level character have zero kinetic energy. Most of the new physics discussed in this paper is related to the property[7] that electric dipoles can be constructed by forming wave functions with coherence between $n=0$ and $n=1$ components. A second peculiarity of the $N=0$ state is that wave functions associated with the K valley are localized in one layer, while wave functions associated with the K' valley are localized in the opposite layer. Layer and valley indices are thus equivalent. It is convenient to use pseudospins to represent both layer (or equivalently valley) and the Landau-level orbital character degrees of freedom. The wave function for an electron in the $N=0$ Landau level is therefore the direct product of a standard guiding center factor and three spinors that capture its dependence on spin, layer, and orbital-Landau-index (n) character. We refer to the final spinor as the orbital spinor, and to the set of eight Landau levels with zero kinetic energy as the bilayer graphene octet.[7] In neutral graphene the octet is half-filled at all magnetic field strengths.

The presence of the octet in bilayers is revealed experimentally by a jump in the quantized Hall conductivity[4] from $-4(e^2/h)$ to $4(e^2/h)$ when the charge density is tuned across neutrality in moderately disordered samples. In a recent paper[7] some of us predicted that quantum Hall effects would appear at all integer filling factors between $\nu=-4$ and $\nu=4$ in samples of quality sufficient[8] to make interactions dominant relative to unintended disorder. Electron-electron interactions acting alone are expected to lift the degeneracy of the bilayer octet and induce gaps at the Fermi level by producing a set of spontaneously broken-symmetry states with spin, valley and orbital pseudospin polarizations. The octet degeneracy lifting is expected[7] to follow a set of Hund's rules in which spin polarization is maximized first, then layer polarization to the greatest extent possible, and finally orbital polarization to the extent allowed by the first two rules. Hall plateaus at all integer filling factors intermediate between $\nu=-4$ and $\nu=4$ have indeed now been discovered in experimental studies of suspended bilayer graphene samples and bilayer graphene on SiO_2/Si substrates,[9,10] opening up the opportunity to study a rich and still relatively unexplored[11,12] family of novel broken-symmetry states. The odd filling factor cases are expected to be most interesting because all three pseu-

dospins are expected to be polarized. The present paper focuses on the physics associated with the competition between layer and orbital pseudospins at Landau levels $\nu=-1$ and $\nu=3$ at field strengths sufficient to produce maximal spin polarization and reduce the importance of Landau-level mixing. In this limit a negative filling factor ν is equivalent to a positive filling factor $\nu+4$ since the two states differ only through the presence in the latter case of inert filled majority spin Landau levels.

In a previous paper[11] we studied the quantum Hall states which occur at $\nu=-3$ and $\nu=1$ in the same strong field regime, emphasizing the key role played by the potential energy difference between graphene layers which we refer to here as the bias potential Δ_B. The $\nu=-3$ ground state at zero bias is an inter-layer coherent state with orbital index $n=0$ that supports counterflow superfluidity. One particularly interesting property of this state is that the superfluid density, the coefficient that relates the counterflow supercurrent to the spatial gradient of interlayer phase, vanishes. Correspondingly, the state's Goldstone mode dispersion is quadratic in wave vector q, in contrast to the linear dispersion found in coherent semiconductor bilayers and in standard superfluids. We also found that the uniform ground state has a long-wavelength instability at any nonzero potential-difference bias $\Delta_B<\Delta_B^{(c)}$ where $\Delta_B^{(c)}$ is the critical bias at which all $N=0$ charge is transferred to a single layer. In Ref. 11, we argued that the instability is probably toward a state in which the direction of the interlayer pseudospin varies in space. For larger bias $\Delta_B>\Delta_B^{(c)}$ the ground state is uninteresting; the charge is completely in one layer (or valley) and in the orbital state $n=0$. The orbital pseudo-spin-wave mode corresponding to transitions between the $n=0$ and $n=1$ orbital states is gapped at a frequency $\omega=\hbar\omega_c^*\Delta_B/\gamma_1$ where γ_1 is the inter-layer tunneling energy in the Bernal stacking. This mode, *which is an intra-Landau level excitation*, has a finite oscillator strength and will absorb[13] electromagnetic radiation. This behavior contrasts with the standard Kohn's theorem[14] behavior in normal 2DEG's which implies that only inter-Landau level excitations produce absorption.

Surprisingly the phase diagrams for $\nu=-1$ and $\nu=3$ states differ qualitatively from the corresponding $\nu=-3$ and $\nu=1$ phase diagrams. The source of the difference is a competition in the $\nu=-1$ case between interaction and single-particle effects which are reinforcing in the $\nu=-3$ case. The end result is that the large Δ_B ground state at $\nu=-1$ places electrons in a coherent combination of $n=0$ and $n=1$ orbital states, and that electric dipoles are consequently spontaneously present in the ground state. This paper analyzes the dependence of bilayer properties on Δ_B and explores some of the consequences of the unusual orbitally ordered dipole state.

At small bias we find that the bilayer's $\nu=-1$ ground state is an inter-layer coherent state, much like the corresponding $\nu=-3$ state except that the coherence is between orbitals with $n=1$ character. This state has a gapless pseudospin wave mode with linear dispersion, like coherent semiconductor bilayers. The state also has a gapped orbital pseudospin collective mode. Because the orbital spinor carries an electric dipole, this mode has a finite oscillator strength and absorbs electromagnetic radiation, again much like the $\nu=-3$ case. This mode should be visible in a microwave spectroscopy experiment.

Interlayer coherence decreases with bias until a new ground state is reached that has both interlayer and orbital coherences. In this mixed state, the low-energy orbital mode is gapless while the interlayer pseudospin modes seem unstable at small wave vector. The collective excitations are highly anisotropic in this phase.

The new physics of the $\nu=-1$ case emerges in its simplest form at still stronger bias potentials. Both orbital levels in the bottom layer are then completely filled while only one of the two top layer Landau levels is filled. Spontaneous orbital coherence then develops in the top layer. This spontaneous orbital coherence leads to a *gapless* orbital pseudospin mode. Some of the properties of this state have been studied independently in a recent paper by Shizuya,[12] who also pointed out that orbital coherence is responsible for the existence of a finite density of electrical dipoles with a net polarization. These dipoles collectively and spontaneously point in some arbitrary direction in the x-y plane. As discussed by Shizuya[12] their orientation can however be controlled by an external electric field parallel to the plane of the bilayer. In this paper, we use an effective pseudospin model to highlight other interesting features of the orbitally coherent state. In particular we demonstrate the presence of a Dzyaloshinskii-Moriya (DM) interaction[15] between orbital pseudospins and show that it leads to an anisotropic softening of the orbital pseudospin mode at a finite wave vector. For strong enough interlayer bias, the DM induces an instability toward a pseudospin spiral state. The orbital pseudospin mode in the high bias regime is gapless and will lead, in the presence of disorder, to strong absorption of electromagnetic waves at very small frequencies.

Our paper is organized in the following way. In Sec. II, we discuss the non-interacting states of the graphene bilayer within a two-band low-energy model. Here we introduce the aspect of the electronic structure that is responsible for interaction and band effects which are competing at $\nu=-1$ and are reinforcing at $\nu=-3$. In Sec. III, we derive the Hamiltonian of the graphene two-dimensional electron gas (2DEG) truncated to $N=0$ levels in the Hartree-Fock approximation. We use this Hamiltonian to derive the equation of motion for the single-particle Green's function in Sec. IV and to obtain the order parameters for the various phases which occur at $\nu=-1$. Section V describes the generalized random-phase approximation (GRPA) [or equivalently the time-dependent Hartree-Fock approximation (TDHFA)] that we use to derive the collective excitations. The phase diagram for $\nu=-1$ as a function of bias is obtained in Sec. VI. We then study the collective excitations of the inter-layer coherent phase in Sec. VII, those of the orbital coherent phase in Sec. VIII, and those of the mixed state in Sec. IX. Finally microwave absorption in the different phases is studied in Sec. X and we conclude with a discussion on the validity of our results when additional tunneling parameters are included in the tight-binding model in Sec. XI.

II. EFFECTIVE TWO-BAND HAMILTONIAN

In a graphene bilayer with Bernal stacking, the two basis atoms of the top layer are denoted by A_1 and B_1 and those of

the bottom layer by A_2 and B_2 with atoms A_1 sitting directly above atoms B_2. The band structure of the bilayer is calculated using a tight-binding model with in-plane nearest-neighbor tunneling (with strength $\gamma_0=2.5$ eV) and A_1-B_2 tunneling (with strength $\gamma_1=0.4$ eV). (For a review of bilayer graphene, see Ref. 16.) The low-energy ($E \ll \gamma_1$) excitations of this model for electrons in the valleys $\xi\mathbf{K}$ with $\mathbf{K}=\frac{2\pi}{a_0}(-\frac{2}{3},0)$ and $\xi=\pm 1$ can be studied by using the effective two-band model developed in Ref. 5. Using the basis $\{|A_2\rangle,|B_1\rangle\}$ for $H^0_{\mathbf{K}}$ and $\{|B_1\rangle,|A_2\rangle\}$ for $H^0_{-\mathbf{K}}$, the effective two-band Hamiltonian derived in Ref. 5 is

$$H^0_{\xi\mathbf{K}}=\begin{pmatrix} -\xi\frac{\Delta_B}{2}+\xi\frac{\Delta_B}{\gamma_1}\frac{1}{2m^*}p_-p_+ & \frac{1}{2m^*}p_-^2 \\ \frac{1}{2m^*}p_+^2 & \xi\frac{\Delta_B}{2}-\xi\frac{\Delta_B}{\gamma_1}\frac{1}{2m^*}p_+p_- \end{pmatrix}, \tag{1}$$

where $p_\pm=p_x\pm ip_y$ and $\mathbf{p}=-i\hbar\nabla$. In this equation, Δ_B is the bias potential between the two layers, the effective mass $m^*=2\hbar^2\gamma_1/3\gamma_0^2a_0^2=0.054m_0$ with m_0 the bare electronic mass, $a_0=\sqrt{3}c$ is the triangular lattice constant and $c=1.42$ Å is the distance between neighboring carbon atoms in the same plane. The kets $|A_2\rangle,|B_1\rangle$ correspond to the atomic sites in different layers that are not directly above one another.

The Hamiltonian of the 2DEG in a perpendicular magnetic field is obtained by making the substitution $\mathbf{p}\to\mathbf{p}+e\mathbf{A}/c\equiv\mathbf{P}/\hbar$ (with $e>0$) in Eq. (1). The vector potential $\mathbf{A}$ is defined such that $\nabla\times\mathbf{A}=B=B\hat{\mathbf{z}}$. In a magnetic field,

$$H^0_{\xi\mathbf{K}}=\begin{pmatrix} -\xi\frac{1}{2}\Delta_B+\xi\beta\Delta_B(1+a^\dagger a) & \hbar\omega_c^*a^2 \\ \hbar\omega_c^*(a^\dagger)^2 & \xi\frac{1}{2}\Delta_B-\xi\beta\Delta_Ba^\dagger a \end{pmatrix}, \tag{2}$$

where we have defined the orbital ladder operators $a=\ell(P_x-iP_y)/\sqrt{2}\hbar$, $a^\dagger=\ell(P_x+iP_y)/\sqrt{2}\hbar$ with the magnetic length $\ell=\sqrt{\hbar c/eB}$ and the parameter $\beta=\hbar\omega_c^*/\gamma_1=6.144\times10^{-3}\,B$(Tesla). The effective cyclotron frequency $\omega_c^*=eB/m^*c$. At zero bias, the Landau levels have energies $E_N^0=\pm\xi\hbar\omega_c^*\sqrt{|N|(|N|+1)}$ with $N=0,\pm1,\pm2,\ldots$

In this paper, we study the phase diagram of the 2DEG in the $N=0$ Landau level. While levels with $|N|>0$ are fourfold degenerate (counting spin and valley quantum numbers), level $N=0$ has an extra *orbital* degeneracy due to the fact that Landau-level orbitals $n=0$ and $n=1$ have zero kinetic energy. The states in $N=0$ are thus member of an octet of Landau levels that are degenerate if we neglect the Zeeman and bias potential energies. We assume that the Zeeman coupling is strong enough to assure maximal spin polarization, which allows this degree-of-freedom to be neglected. The eigenfunctions and corresponding energies for $N=0$ are then given by

$$\begin{pmatrix} 0 \\ h_{0,X}(\mathbf{r}) \end{pmatrix}, \quad E_{K,n=0,X}=\frac{1}{2}\Delta_B, \tag{3}$$

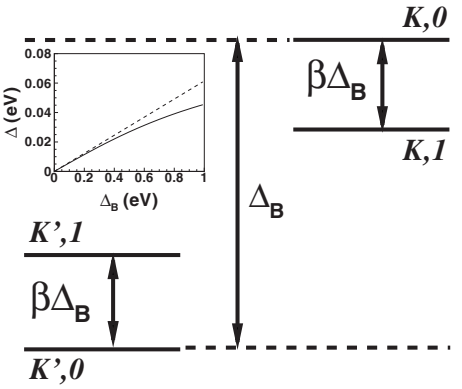

FIG. 1. Noninteracting energy levels in Landau level $N=0$. The inset shows the behavior of the gap evaluated in the original (solid line) and two-band (dashed line) models with bias at $B=10$ T.

$$\begin{pmatrix} 0 \\ h_{1,X}(\mathbf{r}) \end{pmatrix}, \quad E_{K,n=1,X}=\frac{1}{2}\Delta_B-\beta\Delta_B, \tag{4}$$

for the K valley and by

$$\begin{pmatrix} h_{0,X}(\mathbf{r}) \\ 0 \end{pmatrix}, \quad E_{K',n=0,X}=-\frac{1}{2}\Delta_B, \tag{5}$$

$$\begin{pmatrix} h_{1,X}(\mathbf{r}) \\ 0 \end{pmatrix}, \quad E_{K',n=1,X}=-\frac{1}{2}\Delta_B+\beta\Delta_B \tag{6}$$

for the K' valley, using this time the basis $\{|A_2\rangle,|B_1\rangle\}$ for all states. Note that from now on the index n will always refer to the orbital states $n=0,1$ that are part of the same Landau level $N=0$. It is quite clear from these equations that the valley $K(K')$ eigenstates are localized in the top(bottom) layer. For $N=0$, the layer index is thus equivalent to the valley index. (For $|N|>0$, the spinors have different orbital indices n in different layers.) The functions $h_{n,X}(\mathbf{r})=e^{-iXy/\ell^2}\varphi_n(x-X)/\sqrt{L_y}$ are the Landau gauge $[\mathbf{A}=(0,Bx,0)]$ eigenstates of an electron with guiding center X, and $\varphi_n(x)$ is the wave function of a one-dimensional harmonic oscillator. Note that with our choice of gauge, the action of the ladder operators on the states $\varphi_n(x)$ is given by $a^\dagger\varphi_n(x)=i\sqrt{n+1}\varphi_{n+1}(x)$ and $a\varphi_n(x)=-i\sqrt{n}\varphi_{n-1}(x)$.

At finite bias, the parameter $\beta\ll1$ lifts the degeneracy between the two orbital states as we show in Fig. 1. The splitting is however very small. For positive bias, the $n=0$ orbital state in the bottom(top) layer is lower(higher) in energy than the $n=1$ orbital state. The orbital states $n=0,1$ form a two-level system in each valley and we associate them with an *orbital* pseudospin. Similarly, the two states $\pm K$ are associated with a *valley* pseudospin. We remark that the effective two-band model slightly overestimates the gap $\Delta=E_{n=1}-E_{n=0}$ between the $n=0$ and $n=1$ orbital states. The inset in Fig. 1 shows the difference between the gap calculated in the two-band model and in the original four-band system at $B=10$ T. In the region where the DM interaction driven instability occurs, the difference between the two gaps is however very small.

III. HARTREE-FOCK HAMILTONIAN

We now add the Coulomb interaction to the noninteracting Hamiltonian $H^0_{\xi\mathbf{K}}$. We assume that the magnetic field is strong enough so that we can restrict the Hilbert space to the $N=0$ Landau level and neglect Landau level mixing. We also assume the 2DEG to be fully spin polarized (we comment on this later). We write the electron field operator as

$$\Psi_K(\mathbf{r}) = \sum_X \begin{pmatrix} 0 \\ h_{0,X}(\mathbf{r}) \end{pmatrix} c_{K,X,0} + \sum_X \begin{pmatrix} 0 \\ h_{1,X}(\mathbf{r}) \end{pmatrix} c_{K,X,1} \quad (7)$$

and

$$\Psi_{K'}(\mathbf{r}) = \sum_X \begin{pmatrix} h_{0,X}(\mathbf{r}) \\ 0 \end{pmatrix} c_{K',X,0} + \sum_X \begin{pmatrix} h_{1,X}(\mathbf{r}) \\ 0 \end{pmatrix} c_{K',X,1}, \quad (8)$$

so that the Hartree-Fock Hamiltonian is given by (here and in the rest of this paper, we use the convention that repeated indices are summed over)

$$\begin{aligned} H_{HF} &= N_\varphi E_{a,n} \rho^{a,a}_{n,n}(0) \\ &+ N_\varphi \overline{\sum_{\mathbf{q}}} H^{a,b}_{n_1,n_2,n_3,n_4}(\mathbf{q}) \langle \rho^{a,a}_{n_1,n_2}(-\mathbf{q}) \rangle \rho^{b,b}_{n_3,n_4}(\mathbf{q}) \\ &- N_\varphi \sum_{\mathbf{q}} X^{a,b}_{n_1,n_4,n_3,n_2}(\mathbf{q}) \langle \rho^{a,b}_{n_1,n_2}(-\mathbf{q}) \rangle \rho^{b,a}_{n_3,n_4}(\mathbf{q}), \end{aligned} \quad (9)$$

where N_φ is the Landau-level degeneracy and all energies are measured in units of $e^2/\kappa\ell$ where κ is the effective dielectric constant at the position of the graphene layers. The single-particle energies $E_{a,n}$ include capacitive contributions and are defined by

$$E_{a,n} = \frac{1}{2} a \Delta_B - a\beta\Delta_B n + \left[\frac{\tilde{\nu}}{2} \frac{d}{\ell} - \tilde{\nu}_a \frac{d}{\ell} \right], \quad (10)$$

with $\tilde{\nu}_a$ the number of filled levels in valley a, $\tilde{\nu}=\nu+4$ the total number of filled levels, $a,b=\pm 1$ the valley (or equivalently layer) index and $n=0,1$ for the two orbital state indices. In deriving Eq. (9), we have taken into account a neutralizing positive background so that the $\mathbf{q}=0$ contribution is absent in the Hartree term. This convention is indicated by the bar over the summation. Note that for positive bias, the bottom layer (K' valley) is at a lower potential than the top layer (K valley).

The density operators in Eq. (9), are defined by

$$\rho^{a,b}_{n_1,n_2}(\mathbf{q}) = \frac{1}{N_\varphi} \sum_{X_1,X_2} e^{-(i/2)q_x(X_1+X_2)} c^\dagger_{a,X_1,n_1} c_{b,X_2,n_2} \delta_{X_1,X_2+q_y\ell^2}, \quad (11)$$

where $c^\dagger_{a,X_1,n_1}$ creates an electron in state (a,X_1,n_1) in the Landau gauge. The intralayer $(H,X=H^{a,a},X^{a,a})$ and interlayer $(\tilde{H},\tilde{X}=H^{a\neq b},X^{a\neq b})$ Hartree and Fock interactions are given by

$$H_{n_1,n_2,n_3,n_4}(\mathbf{q}) = \frac{1}{q\ell} K_{n_1,n_2}(\mathbf{q}) K_{n_3,n_4}(-\mathbf{q}), \quad (12)$$

$$X_{n_1,n_2,n_3,n_4}(\mathbf{q}) = \int \frac{d\mathbf{p}\ell^2}{2\pi} H_{n_1,n_2,n_3,n_4}(\mathbf{p}) e^{i\mathbf{q}\times\mathbf{p}\ell^2}, \quad (13)$$

and

$$\tilde{H}_{n_1,n_2,n_3,n_4}(\mathbf{q}) = H_{n_1,n_2,n_3,n_4}(\mathbf{q}) e^{-qd}, \quad (14)$$

$$\tilde{X}_{n_1,n_2,n_3,n_4}(\mathbf{q}) = \int \frac{d\mathbf{p}\ell^2}{2\pi} \tilde{H}_{n_1,n_2,n_3,n_4}(\mathbf{p}) e^{i\mathbf{q}\times\mathbf{p}\ell^2}, \quad (15)$$

where $d=3.337$ Å is the inter-layer separation in the Bernal stacking. The form factors which appear here,

$$K_{0,0}(\mathbf{q}) = \exp\left(\frac{-q^2\ell^2}{4}\right), \quad (16)$$

$$K_{1,1}(\mathbf{q}) = \exp\left(\frac{-q^2\ell^2}{4}\right)\left(1 - \frac{q^2\ell^2}{2}\right), \quad (17)$$

$$K_{1,0}(\mathbf{q}) = \left(\frac{(q_y + iq_x)\ell}{\sqrt{2}}\right)\exp\left(\frac{-q^2\ell^2}{4}\right), \quad (18)$$

$$K_{0,1}(\mathbf{q}) = \left(\frac{(-q_y + iq_x)\ell}{\sqrt{2}}\right)\exp\left(\frac{-q^2\ell^2}{4}\right), \quad (19)$$

capture the character of the two different orbital states. Detailed expressions for the Hartree and Fock interactions parameters are given in Appendix A.

IV. ORDER PARAMETERS AT INTEGER FILLINGS

The states with no pseudospin texture at integer filling factors have uniform electronic density and density matrices that vanish for $\mathbf{q}\neq 0$. Letting $\langle \rho^{a,b}_{n_1,n_2}(\mathbf{q}=0)\rangle \to \langle \rho^{a,b}_{n_1,n_2}\rangle$, the Hamiltonian of Eq. (9) reduces to

$$H_{HF} = N_\varphi E_{a,n} \rho^{a,a}_{n,n} - N_\varphi X^{a,b}_{n_1,n_4,n_3,n_2}(0) \langle \rho^{a,b}_{n_1,n_2}\rangle \rho^{b,a}_{n_3,n_4}. \quad (20)$$

These order parameters are conveniently calculated by defining the time-ordered Matsubara Green's function

$$G^{a,b}_{n_1,n_2}(\tau) = -\frac{1}{N_\varphi} \sum_X \langle T_\tau c_{a,n_1,X}(\tau) c^\dagger_{b,n_2,X}(0)\rangle, \quad (21)$$

since, at time zero, we have

$$G^{a,b}_{n_1,n_2}(\tau = 0^-) = \langle \rho^{b,a}_{n_2,n_1}\rangle \quad (22)$$

and by definition

$$\langle \rho^{a,a}_{n,n}\rangle = \nu_{a,n}, \quad (23)$$

where $\nu_{a,n}$ is the filling factor of the state (a,n).

In the Hartree-Fock approximation, the equation of motion for the single-particle Green's function is

$$[\hbar i\omega_n - (E_{a,n_1} - \mu)] G^{a,b}_{n_1,n_2}(\omega_n) + U^{a,c}_{n_1,n_3} G^{c,b}_{n_3,n_2}(\omega_n) = \hbar \delta_{a,b} \delta_{n_1,n_2}, \quad (24)$$

where ω_n is a fermionic Matsubara frequency and

$$U^{a,c}_{n_1,n_3} = X^{a,c}_{n,n_3,n_1,n'}(0)\langle\rho^{c,a}_{n,n'}\rangle. \tag{25}$$

The system of Eqs. (24) can be solved in an iterative way by using some initial values for the parameters $\{\langle\rho^{b,a}_{n_2,n_1}\rangle\}$. In Ref. 7, we solved this equation keeping valley, orbital, and spin indices. We showed that the solutions of the Hartree-Fock equations for the balanced bilayer ($\Delta_B=0$) follow a Hund's rules behavior. The spin polarization is maximized first, then the layer polarization is maximized to the greatest extent possible, and finally the orbital polarization is maximized to the extent allowed by the first two rules. In the absence of bias, the ordering of the first four states (with spin up) is given by

$$|S,0\rangle = \frac{1}{\sqrt{2}}|K,0\rangle + \frac{1}{\sqrt{2}}|K',0\rangle, \tag{26}$$

$$|S,1\rangle = \frac{1}{\sqrt{2}}|K,1\rangle + \frac{1}{\sqrt{2}}|K',1\rangle, \tag{27}$$

$$|AS,0\rangle = \frac{1}{\sqrt{2}}|K,0\rangle - \frac{1}{\sqrt{2}}|K',0\rangle, \tag{28}$$

$$|AS,1\rangle = \frac{1}{\sqrt{2}}|K,1\rangle - \frac{1}{\sqrt{2}}|K',1\rangle, \tag{29}$$

in this order. The next four states follow the same order but with spin down. The occupation of these eight states are given by the filling factor ν ranging from $\nu=-3$ (state $|S,0\rangle$ with spin up fully filled) to $\nu=+4$ (all eight states filled). We remark that the four states given above correspond to a particular choice of phase for the ground state. For example, when the U(1) symmetry of the interlayer pseudospin is not broken at $\nu=-3$, all orientations of this pseudospin in the x-y plane lead to the same energy. When we break the U(1) symmetry in our Hartree-Fock calculation and choose $|S,0\rangle$ for the ground state (at zero bias), then the interlayer exchange interaction induces a gap between the states $|S,0\rangle$ and $|AS,0\rangle$.

V. COLLECTIVE MODES IN THE GENERALIZED RANDOM-PHASE APPROXIMATION

In order to compute the collective excitations, we define the two-particle Matsubara Green's function

$$\chi^{a,b,c,d}_{n_1,n_2,n_3,n_4}(\mathbf{q},\tau) = -N_\varphi\langle T_\tau\rho^{a,b}_{n_1,n_2}(\mathbf{q},\tau)\rho^{c,d}_{n_3,n_4}(-\mathbf{q},0)\rangle + N_\varphi\langle\rho^{a,b}_{n_1,n_2}(\mathbf{q})\rangle\langle\rho^{c,d}_{n_3,n_4}(-\mathbf{q})\rangle, \tag{30}$$

where again $n_i=0,1$ are orbital indices and a,b,c,d are valley indices. To derive the equation of motion for these response functions in the generalized random-phase approximation (GRPA), we proceed in the following way. We first derive the equation of motion for χ in the Hartree-Fock Approximation (HFA) using the Heisenberg equation of motion

$$\hbar\frac{\partial}{\partial\tau}(\dots) = [H-\mu N,(\dots)], \tag{31}$$

where H is the Hamiltonian of Eq. (9) with the averages removed, μ is the chemical potential and N the number operator (not to be confused with the Landau-level index). After evaluating the commutators, we linearize the resulting equation by writing $\rho(\mathbf{q})\to\langle\rho(\mathbf{q})\rangle_{HFA}+\delta\rho(\mathbf{q})$. We get the GRPA equations of motion by keeping the terms up to linear order in $\delta\rho(\mathbf{q})$. In the homogeneous states at integer fillings, $\langle\rho(\mathbf{q})\rangle_{HF}=\langle\rho(\mathbf{q})\rangle_{HF}\delta_{\mathbf{q},0}$, so that we get the set of equations

$$[i\hbar\Omega_n-(E_{b,n_2}-E_{a,n_1})]\chi^{(0)a,b,c,d}_{n_1,n_2,n_3,n_4}(\mathbf{q},\Omega_n) = \hbar\langle\rho^{a,d}_{n_1,n_4}\rangle\delta_{n_2,n_3}\delta_{b,c} - \hbar\langle\rho^{c,b}_{n_3,n_2}\rangle\delta_{a,d}\delta_{n_1,n_4} + X^{a,b'}_{n'_1,n_1,n'_3,n'_2}(0)\langle\rho^{a,b'}_{n'_1,n'_2}\rangle\chi^{(0)b',b,c,d}_{n'_3,n_2,n_3,n_4}(\mathbf{q},\Omega_n) - X^{a',b}_{n'_1,n'_4,n_2,n'_2}(0)\langle\rho^{a',b}_{n'_1,n'_2}\rangle\chi^{(0)a,a',c,d}_{n_1,n'_4,n_3,n_4}(\mathbf{q},\Omega_n), \tag{32}$$

and

$$\chi^{a,b,c,d}_{n_1,n_2,n_3,n_4}(\mathbf{q};\Omega_n) = \chi^{(0)a,b,c,d}_{n_1,n_2,n_3,n_4}(\mathbf{q};\Omega_n) + \frac{1}{\hbar}\chi^{(0)a,b,e,e}_{n_1,n_2,n_5,n_6}(\mathbf{q};\Omega_n)H^{e,g}_{n_5,n_6,n_7,n_8}(\mathbf{q})\times\chi^{g,g,c,d}_{n_7,n_8,n_3,n_4}(\mathbf{q};\Omega_n) - \frac{1}{\hbar}\chi^{(0)a,b,e,f}_{n_1,n_2,n_5,n_6}(\mathbf{q};\Omega_n)X^{e,f}_{n_5,n_8,n_7,n_6}(\mathbf{q})\times\chi^{f,e,c,d}_{n_7,n_8,n_3,n_4}(\mathbf{q};\Omega_n), \tag{33}$$

where Ω_n is a bosonic Matsubara frequency. The retarded response functions are obtained, as usual, by taking the analytic continuation $i\Omega_n\to\omega+i\delta$.

By defining super indices $A,B=1,2,3,\dots,16$ representing the combinations $(a,n_1;b,n_2),(c,n_3;d,n_4)$, etc., we can represent the response functions and interactions matrices as 16×16 matrices and then write the GRPA equation in the matrix form,

$$[(\omega+i\delta)I-F(\mathbf{q})]\chi(\mathbf{q},\omega) = B(\mathbf{q}), \tag{34}$$

where B,I,F,χ are 16×16 matrices (with I the unit matrix). The matrices $F(\mathbf{q})$ and $B(\mathbf{q})$ depend on the $\langle\rho^{b,a}_{n_2,n_1}\rangle's$ evaluated in the HFA. We will give later the precise form of these matrices for the phases studied in this paper.

The frequencies of the collective excitations are given by the eigenvalues of the matrix $F(\mathbf{q})$. There are in total 4 zero

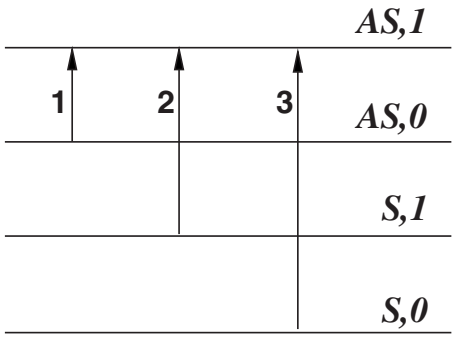

FIG. 2. At $\nu=-1$, the first three energy states of the Hartree-Fock Hamiltonian are filled and the only possible transitions are those indicated by the three arrows. The frequency of these transitions corresponds to the frequency of the collective excitations calculated in the GRPA in the limit in which the wave vector $q\to\infty$. We illustrate here the case of zero bias.

modes, corresponding to unphysical intralevel transitions, and 12 nonzero modes corresponding to inter-level transitions. The latter occur in six positive-negative energy pairs, corresponding to excitation and deexcitation partners. Of the six collective excitations identified in this way, three are Pauli-blocked at $\nu=-1$ and appear in our calculations as dispersionless modes that have zero weight in all physical response properties. The three remaining excitation modes are physical and for $\nu=-1$ correspond to the interaction-coupled transitions indicated in Fig. 2. Note that, in the limit $q\to\infty$, $H^{e,g},X^{e,f}\to 0$ so that Eq. (33) gives $\chi\to\chi^0$. In this limit, the collective mode frequencies correspond to transitions between eigenstates of the Hartree-Fock Hamiltonian H_{HF} as illustrated in Fig. 2 for the case $\nu=-1$ and zero bias. The energy of these eigenstates include the noninteracting energies and the self-energy corrections. The $\omega(\mathbf{q}=0)$ limit of these same modes, however, also includes the polarization and excitonic corrections that, in a Feynman diagram description of the GRPA, are captured by bubble and ladder diagram summations. These effects make the modes dispersive.

VI. PHASE DIAGRAM AT FILLING FACTOR $\nu=-1$

The properties of the ground state at $\nu=-3$ have been studied in detail in Ref. 11. At zero bias, the ground state has all electrons in the $|S,0\rangle$ state and can be described as an XY layer-pseudospin ferromagnet with orbital character $n=0$. The bias Δ_B acts as an effective external magnetic field that forces the layer pseudospins out of the x-y plane. Above a critical bias $\Delta_B^{(c)}$, all electrons are in the bottom layer and the layer pseudospin is correspondingly fully polarized. The ground state is then given by $|K',0\rangle$ and is unchanged if the bias is further increased. The $\nu=-1$ state on which we focus here differs from the $\nu=-3$ state because of a competition between single-particle and interaction energy effects which emerges only in the former case. As illustrated in Fig. 1, single-particle effects captured by the bilayer effective Hamiltonian favor occupation of the $n=1$ orbital when three of the octet's eight levels are occupied ($\nu=-1$). Note that this tendency is independent of the sign of Δ_B. Exchange interactions, on the other hand, always favor a state in which as many $n=0$ orbitals as possible are occupied. As we explain below, a compromise is reached by forming a state with coherence between $n=0$ and $n=1$ orbitals. This physics is enriched by the same tendency toward interlayer coherence which occurs at $\nu=-3$ and[1] in semiconductor bilayers. Indeed, our calculations show that the phase diagram at $\nu=-1$ is much more complex than at $\nu=-3$. YAFIS: Thus, because the contribution $\beta\Delta_B$ has a different sign in both layers, there is no electron-hole symmetry between the first four spin polarized states.

A. Interlayer-coherent state

At zero bias, numerical solution of the HFA equations leads to occupied $|S,0\rangle$, $|S,1\rangle$ and $|AS,0\rangle$ states. The order parameters are then given by

$$\nu_{K,0}=\nu_{K',0}=1,$$

$$\nu_{K,1}=\nu_{K',1}=\frac{1}{2},$$

$$\langle\rho_{1,1}^{K,K'}\rangle=\langle\rho_{1,1}^{K',K}\rangle=\frac{1}{2}. \tag{35}$$

The ground state is an XY layer-pseudospin ferromagnet with orbital character $n=1$. The Hamiltonian is invariant with respect to the orientation of the pseudospins in the x-y plane so that this phase supports a Goldstone mode. The choice of phase in Eq. (35) has the pseudospins pointing along the x axis. At finite bias $\Delta_B<\Delta_B^{(1)}$, the pseudospins are pushed out the x-y plane i.e., the two layers have unequal population. The occupation of the four states is in this case

$$\nu_{K,0}=\nu_{K',0}=1, \tag{36}$$

and

$$\nu_{K,1}=1-\nu_{K',1}=\frac{1}{2}\left(1-\frac{\Delta_B}{\Delta_B^{(1)}}\right), \tag{37}$$

with inter-layer coherence reflected by

$$\langle\rho_{1,1}^{K,K'}\rangle=\langle\rho_{1,1}^{K',K}\rangle=\sqrt{\nu_{K,1}-\nu_{K,1}^2}. \tag{38}$$

We define the critical bias $\Delta_B^{(1)}$ as the bias at which the interlayer coherence $\langle\rho_{1,1}^{K,K'}\rangle=0$. It is given by

$$\Delta_B^{(1)}=\frac{-3x_7(0)+2\tilde{x}_{16}(0)+2\dfrac{d}{\ell}}{2-4\beta}, \tag{39}$$

where the Fock interactions $x_i(\mathbf{q})$ and $\tilde{x}_i(\mathbf{q})$ are defined in Appendix A. As an example, for $B=10$ T, $\Delta_B^{(1)}=0.00205e^2/\kappa\ell$.

The energy of this interlayer-coherent state (ICS) for $\Delta_B<\Delta_B^{(1)}$ is

$$\frac{E_{HF}^{(1)}}{N_0} = \frac{1}{3}\Delta_B(1-2\beta)\langle P_{z,1}\rangle - \frac{1}{3}x_1(0) - \frac{1}{3}x_7(0) - \frac{1}{12}x_{16}(0) + \frac{1}{3}\left(\frac{d}{\ell} - x_{16}(0)\right)\langle P_{z,1}\rangle^2 - \frac{1}{3}\tilde{x}_{16}(0)\langle \mathbf{P}_{\perp,1}\rangle^2, \quad (40)$$

where N_0 is the number of electrons and the components of the layer pseudospin are given by

$$\langle P_{z,1}\rangle = \frac{\nu_{K,1} - \nu_{K',1}}{2} = -\frac{1}{2}\frac{\Delta_B}{\Delta_B^{(1)}}, \quad (41)$$

$$\langle \mathbf{P}_{\perp,1}\rangle^2 = \langle P_{x,1}\rangle^2 + \langle P_{y,1}\rangle^2 = |\langle \rho_{1,1}^{K,K'}\rangle|^2, \quad (42)$$

with the convention that pseudospin up is state $|K,1\rangle$ while pseudospin down is state $|K',1\rangle$.

B. Interorbital-coherent state

The HFA equations have a separate set of solutions, favored at larger bias voltages, in which the lower layer is maximally occupied, and the ground state has upper-layer orbital coherence instead of interlayer coherence. This solution has

$$\nu_{K',0} = \nu_{K',1} = 1, \quad (43)$$

$$\nu_{K,1} = 1 - \nu_{K,0} = \frac{\Delta_B}{\Delta_B^{(2)}}, \quad (44)$$

and inter-orbital coherence is signaled by the density-matrix components

$$\langle \rho_{0,1}^{K,K}\rangle = \langle \rho_{1,0}^{K,K}\rangle = \sqrt{\nu_{K,1} - \nu_{K,1}^2}. \quad (45)$$

Here

$$\Delta_B^{(2)} = \frac{x_4(0)}{2\beta} \quad (46)$$

is the critical bias above which all charges in the upper layer are transferred to state $|K,1\rangle$ and the orbital coherence is lost. In a pseudospin model with the convention: pseudospin up for state $|K,0\rangle$ and pseudospin down for state $|K,1\rangle$, the orbital pseudospin components are given by

$$\langle S_{z,K}\rangle = \frac{\nu_{K,0} - \nu_{K,1}}{2}, \quad (47)$$

$$\langle \mathbf{S}_{\perp,1}\rangle = \langle S_{x,1}\rangle\hat{\mathbf{x}} + \langle S_{y,1}\rangle\hat{\mathbf{y}}, \quad (48)$$

$$\langle S_{+,K}\rangle = \langle S_{x,K}\rangle + i\langle S_{y,K}\rangle = \langle \rho_{0,1}^{K,K}\rangle. \quad (49)$$

This orbital-coherent phase has all pseudospins tilted slightly away from the z axis by an angle

$$\cos\,\theta_B = 1 - 2\frac{\Delta_B}{\Delta_B^{(2)}}. \quad (50)$$

At the critical bias $\Delta_B^{(2)}$, $\theta_B = \pi$. This critical bias $\Delta_B^{(2)}$ is very large; at $B = 10$ T, $\Delta_B^{(2)} \approx 5e^2/\kappa\ell$ which is near the limit of validity of the effective two-band model i.e., $\hbar\omega_c < \gamma_1$. For $\Delta_B > \Delta_B^{(2)}$, all electrons are in state $|K,1\rangle$ and there is no further change with bias of the ground state.

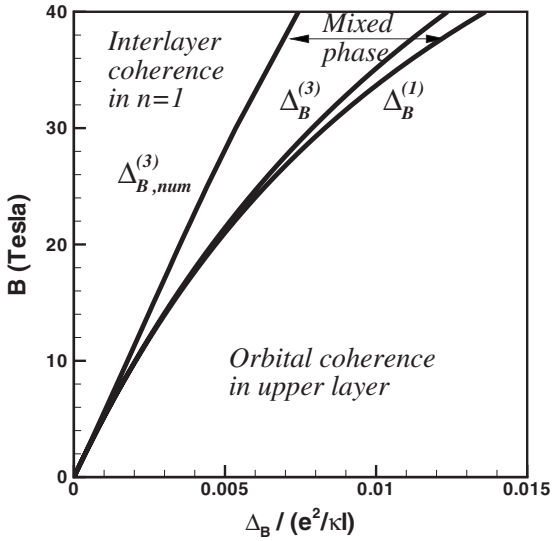

FIG. 3. Phase diagram of the 2DEG in a graphene bilayer at $\nu = -1$.

The orbital-coherent state (OCS) has an energy given by

$$\frac{E_{HF}^{(2)}}{N_0} = \frac{1}{3}\left[-(1-\beta)\frac{\Delta_B}{2} + \beta\Delta_B\langle S_{z,K}\rangle\right] + \frac{1}{12}\frac{d}{\ell} - \frac{5}{24}[x_1(0) + x_{16}(0) + 2x_7(0)] - \frac{1}{6}[x_1(0) - x_{16}(0)]\langle S_{z,K}\rangle - \frac{1}{6}[x_1(0) + x_{16}(0) - 4x_7(0)]\langle S_{z,K}\rangle^2 - \frac{1}{3}x_4(0)\langle \mathbf{S}_{\perp,K}\rangle^2. \quad (51)$$

This energy is independent of the azimuthal angle φ of the pseudospin vector. We can thus, without loss of generality, take $\langle \rho_{0,1}^{K,K}\rangle$ as real.

C. Mixed state

Equations (40) and (51) give $E_{HF}^{(2)} < E_{HF}^{(1)}$ above a critical bias $\Delta_B^{(3)} < \Delta_B^{(1)}$. For biases $\Delta \in [\Delta_B^{(3)}, \Delta_B^{(1)}]$, a mixed state with both interorbital *and* interlayer coherence would be lower in energy than a state with only interlayer coherence. Solving the full Hartree-Fock equations, we find that the crossover from the interlayer coherent state to the interorbital coherent state occurs continuously via an intermediate state with both orders. The boundaries of the intermediate phase must be determined numerically. We find that the boundaries of this mixed state (MS) are given on the left by a new critical bias $\Delta_{B,num}^{(3)} < \Delta_B^{(3)}$ and on the right by $\Delta_B^{(1)}$. The intermediate phase region broadens with magnetic field as can be seen in Fig. 3.

Figure 4 shows the evolution of the inter-layer coherence $\langle \rho_{1,1}^{K,K'}\rangle$ and the orbital coherence $\langle \rho_{0,1}^{K,K}\rangle$ with bias at magnetic

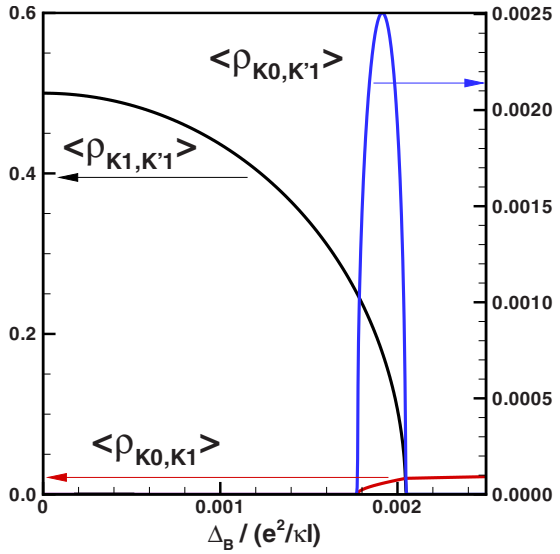

FIG. 4. (Color online) Evolution of the inter-layer $\langle\rho_{1,1}^{K,K'}\rangle$ and interorbital $\langle\rho_{0,1}^{K,K}\rangle$ coherences (left axis) with bias at filling factor $\nu=-1$ and magnetic field $B=10$ T. On the right axis, one of the nonzero coherences $\langle\rho_{0,1}^{K,K'}\rangle$ in the mixed state.

field $B=10$ T. The orbital coherence sets in before the inter-layer coherence decreases to zero thus creating the mixed state region identified in this figure by a nonzero value of the density-matrix component $\langle\rho_{0,1}^{K,K'}\rangle$. [Note that $\langle\rho_{0,1}^{K,K}\rangle$ is not given by Eq. (45) in the mixed state.] The coherences $\langle\rho_{0,1}^{K,K'}\rangle$ and $\langle\rho_{1,0}^{K,K'}\rangle$, which involve a mixing of valley and as well as orbital indices, are nonzero only in the intermediate mixed-state region of the phase diagram. All density-matrix components vary continuously with interlayer bias.

As can be seen from Figs. 3 and 4, the orbital-coherent phase starts at $\Delta_B^{(1)}$ with a finite orbital coherence $\langle\rho_{0,1}^{K,K}\rangle$. Were it not for the presence of the interlayer-coherent and mixed states, $\langle\rho_{0,1}^{K,K}\rangle$ would start at zero bias and be given by Eq. (45) for all biases. The mixed and interlayer coherent states are confined to relatively small inter-layer bias voltages; at larger values of Δ_B the ground state is a relatively simple state with only orbital coherence. The exploration of collective excitation properties of this state is one key objective of this paper.

VII. COLLECTIVE MODES IN THE INTER-LAYER COHERENT STATE

The density-matrix equations of motions which describe the three $\nu=-1$ spin-diagonal dispersive collective modes are given in Appendix B. The resulting GRPA dispersions for the three collective modes are shown in Fig. 5 for zero bias and a magnetic field of $B=10$ T. In the limit $q\to\infty$, the frequencies of the dispersive modes correspond to transitions between the HFA energy levels indicated in Fig. 2 as expected. Mode 2 in Fig. 5 is a Goldstone mode consisting of a precession of the inter-layer pseudospin $\mathbf{P}_1$ around the x axis. We refer to it as the inter-layer pseudospin mode (IPM). Mode 1 is an orbital pseudospin mode (OPM) consisting of a

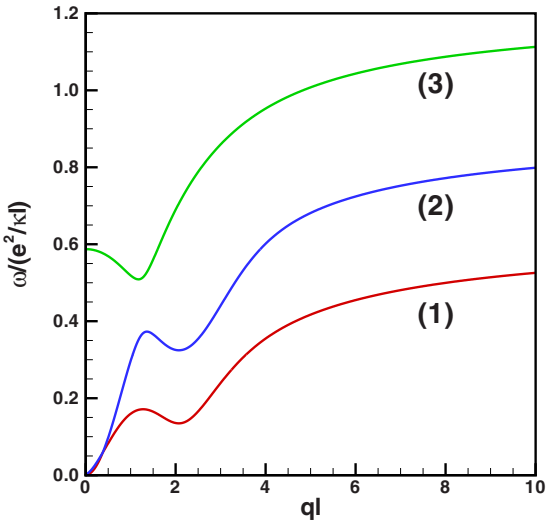

FIG. 5. (Color online) Dispersion relations of the collective modes at $\nu=-1$ in the interlayer coherent phase at zero bias and for $B=10$ T. The numbers refer to the transitions indicated in Fig. 2.

precession of the orbital pseudospins around their local equilibrium position. Mode 3 involves both a layer and orbital pseudospin flip and has a large gap. At finite bias, the 3 dispersive modes in Fig. 2 are coupled together while at zero bias, modes 2 and 3 completely decouple from mode 1 as [see Eq. (B6) in Appendix B].

The OPM at zero bias has a gap given by (see Appendix B)

$$\omega_{OPM}(0)=\frac{1}{2}[x_1(0)-\tilde{x}_1(0)-x_{16}(0)+\tilde{x}_{16}(0)]. \quad (52)$$

This gap is small but visible in Fig. 6. We find numerically, that as the bias is increased, the gap $\omega_{OPM}(0)$ decreases until it reaches zero at the phase boundary of the mixed state.

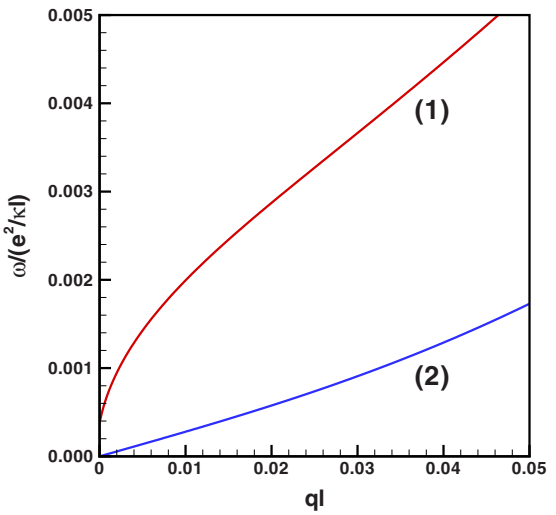

FIG. 6. (Color online) Long-wavelength (small q) dispersion relation of the collective modes in the interlayer coherent phase at $\nu=-1$ for zero bias and for $B=10$ T. Mode 1 is the orbital pseudospin mode while mode 2 is the inter-layer pseudospin mode.

The dispersion of the IPM is linear in q for $q\ell < d/\ell$ (with $d/\ell \approx 0.04$ for $B=10$ T) as in a semiconductor bilayer.[17] An important distinction between the two systems is that the ratio d/ℓ is very small in bilayer graphene due to the proximity of the two graphene layers. This makes the interlayer Hartree and Fock interactions not much different from the intralayer interactions. In consequence, the SU(2) symmetry of the interlayer pseudospin is only weakly broken at zero bias. That explains why the IPM crosses rapidly from the linear to the quadratic behavior with increasing wave vector. The smallness of d/ℓ also causes the transition from the interlayer to the interorbital states to occur at very small bias as can be seen from Fig. 4 since the bias energy can easily overcome the capacitive energy.

The linearity of the IPM differs qualitatively from the $\nu=-3$, case for which we found[11] an IPM with q^2 dispersion and a gapless OPM. At $\nu=-3$ and zero bias, the $|S,0\rangle$ level is filled. The q^2 IPM dispersion in that case occurs because the possibility of mixing $n=1$ wave functions with $|AS,0\rangle$ wave functions in excited states allows the interlayer phase stiffness to vanish. At $\nu=-1$, it is not possible to make the corresponding admixture.

In pseudospin language, a finite bias pushes the layer pseudospins $\mathbf{P}_1$ out of the x-y plane but the Hamiltonian of the system remains independent of the orientation of the perpendicular component of these pseudospins in the x-y plane. The IPM therefore remains gapless for $\Delta_B < \Delta_{B,num}^{(3)}$. It acquires a gap in the mixed and OCS. At filling factor $\nu=-3$, the interlayer-pseudospin mode becomes unstable at finite bias. This indicates that the uniform interlayer-coherent state cannot in fact be the ground state at finite bias. We see no such instability at $\nu=-1$.

In the absence of a bias, Eq. (B6) shows that modes 2 and 3 are coupled through N and J. These interactions involves the Coulomb interaction matrix elements $\hat{X}_{0,1,1,1}(\mathbf{q})$ and $\hat{H}_{0,1,1,1}(\mathbf{q})$ (see Appendix A for their definitions). These interactions do not conserve total $n=0$ or $n=1$ quantum numbers. Such interactions do not occur in usual semiconductor 2DEG where spin and layer pseudospin indices are conserved.

VIII. COLLECTIVE MODES IN THE ORBITAL COHERENT STATE

In this section, we consider collective excitations of the orbital coherent state (OCS) which is the ground state in the region $\Delta_B^{(1)} < \Delta_B < \Delta_B^{(2)}$, which covers the large region of bias voltages from small values to the largest values for which the two-band effective model applies. The occurrence of the interesting OCS state at high bias voltages is a consequence of competition between single-particle and interaction effects as explained earlier. By studying its collective interactions we reveal a Dzyaloshinskii-Moriya (DM) interaction between orbital pseudospins and demonstrate that for large bias voltages it drives an instability to an orbital pseudospin spiral state.

A. Electric dipole density

The fact that $\langle \rho_{0,1}^{K,K} \rangle \neq 0$ in the OCS implies that there is a finite density of electric dipoles in this phase as first pointed out in Ref. 12. To show this, we write the total electronic density (including the two valleys) as

$$n(\mathbf{q}) = n_K(\mathbf{q}) + n_{K'}(\mathbf{q}), \tag{53}$$

where

$$n_K(\mathbf{q}) = N_\varphi \sum_{i,j=0,1} K_{i,j}(-\mathbf{q}) \rho_{i,j}^{K,K}(\mathbf{q}) \tag{54}$$

The functions $K_{i,j}(\mathbf{q})$ are defined in Eqs. (16)–(19). In our pseudospin language for the orbital states, we have the relations (for the K valley)

$$\rho^K(\mathbf{q}) = \rho_{0,0}^{K,K}(\mathbf{q}) + \rho_{1,1}^{K,K}(\mathbf{q}), \tag{55}$$

$$\rho_z^K(\mathbf{q}) = \frac{1}{2}[\rho_{0,0}^{K,K}(\mathbf{q}) - \rho_{1,1}^{K,K}(\mathbf{q})], \tag{56}$$

$$\rho_+^K(\mathbf{q}) = \rho_{0,1}^{K,K}(\mathbf{q}) = \rho_x^K(\mathbf{q}) + i\rho_y^K(\mathbf{q}) \tag{57}$$

and so the density operator in the K valley can be written as

$$n_K(\mathbf{q}) = N_\varphi \left(1 - \frac{q^2\ell^2}{4}\right) \bar{\rho}_K(\mathbf{q}) + N_\varphi \left(\frac{q^2\ell^2}{2}\right) \bar{\rho}_{K,z}(\mathbf{q}) - N_\varphi \sqrt{2} i q_x \ell \bar{\rho}_{K,x}(\mathbf{q}) + N_\varphi \sqrt{2} i q_y \ell \bar{\rho}_{K,y}(\mathbf{q}), \tag{58}$$

where we have defined $\bar{\rho}_K(\mathbf{q}) = \exp(-q^2\ell^2/4)\rho^K(\mathbf{q})$ and similarly for $\bar{\rho}_{K,i}$ with $i=x,y,z$.

Now, if the 2DEG is in an external electric field $\mathbf{E}(\mathbf{r}) = -\nabla\phi(\mathbf{r})$, we have for the coupling Hamiltonian

$$H_{ext} = -e\int d\mathbf{r} n(\mathbf{r})\phi(\mathbf{r}) = -\frac{e}{S} N_\varphi \sum_{j=K,K'} \sum_{\mathbf{q}} e^{i\mathbf{q}\cdot\mathbf{r}} \left[\left(1 - \frac{q^2\ell^2}{4}\right) \bar{\rho}_j(-\mathbf{q}) + \left(\frac{q^2\ell^2}{2}\right) \bar{\rho}_{j,z}(-\mathbf{q}) - \sqrt{2} i (q_x \ell \bar{\rho}_{j,x}(-\mathbf{q}) - q_y \ell \bar{\rho}_{j,y}(-\mathbf{q})) \right] \phi(\mathbf{q}). \tag{59}$$

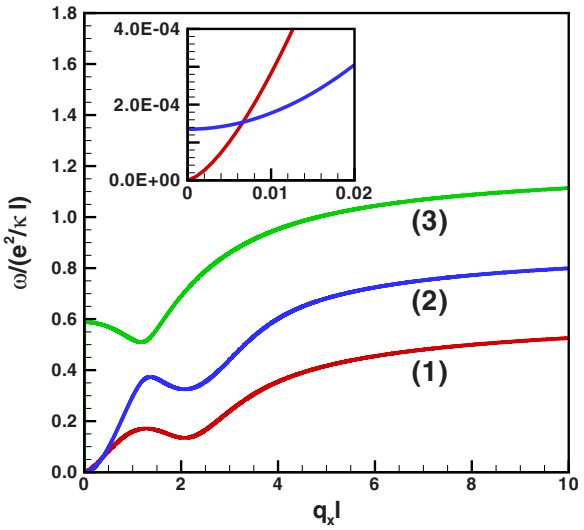

FIG. 7. (Color online) Dispersion relations of the collective modes along q_x in the orbital-coherent state at filling factor $\nu=-1$, bias $\Delta_B=0.0022\ e^2/\kappa\ell$ and magnetic field $B=10$ T. Mode 1 is the Goldstone mode due to orbital coherence. Modes 2 and 3 involve an interlayer transition and are gapped. The inset shows the dispersion of mode 1 (gapless) and mode 2 (gapped) at small $q_x\ell$.

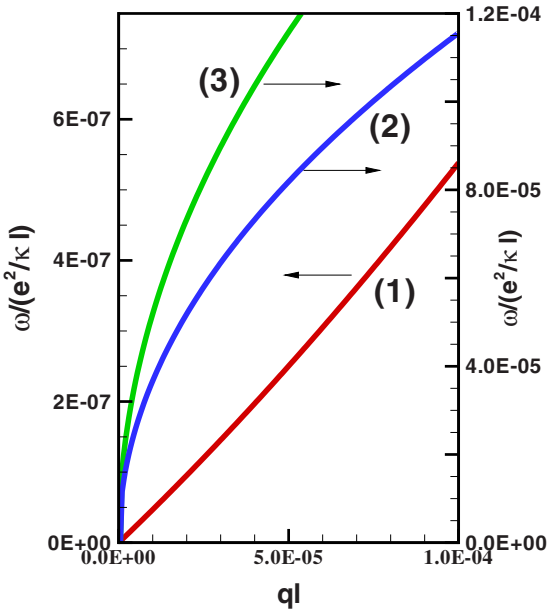

FIG. 8. (Color online) Dispersion relations of the collective modes in the orbital-coherent phase at filling factor $\nu=-1$, bias $\Delta_B=0.0022\ e^2/\kappa\ell$ and magnetic field $B=10$ T. Curve (1) $q_y=0$; curve (2) $q_x=q_y$; and curve (3) $q_x=0$.

With the electric field in the plane of the 2DEG, this coupling can be written, in real space, as

$$H_{ext} = -eN_\varphi \sum_{j=K,K'} \int d\mathbf{r}\Bigg[\bar{\rho}_j(\mathbf{r})\phi(\mathbf{r}) - \frac{1}{4}(\bar{\rho}_j(\mathbf{r})\ell^2 - 2\bar{\rho}_{j,z}(\mathbf{r})\ell^2) \times(\nabla\cdot\mathbf{E}(\mathbf{r}))\Bigg] + \sqrt{2}\ell\int d\mathbf{r}[\bar{\rho}_{j,x}(\mathbf{r})E_x(\mathbf{r}) - \bar{\rho}_{j,y}(\mathbf{r})E_y(\mathbf{r})]. \tag{60}$$

The inter-orbital coherence is zero in the K' valley and so $\langle\bar{\rho}_{K',x}\rangle, \langle\bar{\rho}_{K',y}\rangle = 0$. Equation (60) implies that the dipole density in the 2D plane is

$$\langle\bar{\mathbf{d}}_K(\mathbf{r})\rangle = -e\sqrt{2}\ell N_\varphi(\langle\bar{\rho}_{K,x}(\mathbf{r})\rangle\hat{\mathbf{x}} - \langle\bar{\rho}_{K,y}(\mathbf{r})\rangle\hat{\mathbf{y}}), \tag{61}$$

or

$$\langle\mathbf{d}_K(\mathbf{q})\rangle = -e\sqrt{2}\ell N_\varphi e^{-q^2\ell^2/4}\times(\langle\rho_{K,x}(\mathbf{q})\rangle\hat{\mathbf{x}} - \langle\rho_{K,y}(\mathbf{q})\rangle\hat{\mathbf{y}}). \tag{62}$$

The orientation of the dipole density is set by the phase of the density-matrix component $\langle\rho_{0,1}^{K,K}(\mathbf{r})\rangle$ which specifies the phase of the spontaneously established coherence between $n=0$ and $n=1$ orbitals in the ground state. For our choice of the spontaneously established phase of $\langle\rho_{0,1}^{K,K}(\mathbf{r})\rangle$ in Eq. (45), the dipoles are oriented along the x axis. Because the K' valley (bottom layer) Landau levels are maximally filled, there is no interorbital coherence and therefore no contribution to the electric-dipole density from the K' valley.

B. Effective pseudospin model

Collective modes dispersions for the OCS are plotted in Fig. 7. For relatively small values of Δ_B they are very similar to those represented in Fig. 5 for the ICS; the main changes occur at small wave vector as can be seen in the inset of Fig. 7. The interlayer pseudospin mode is gapped in the OCS while the orbital pseudospin mode is gapless, with a very anisotropic dispersion as shown in Fig. 8. We now discuss the physics of the orbital pseudospin mode.

At finite wave vector $\mathbf{q}$, the orbital pseudospin mode (OPM) corresponds to a precession of the orbital pseudospins around their equilibrium orientation in the ground state as illustrated in Fig. 9. The ground state is described by spinors

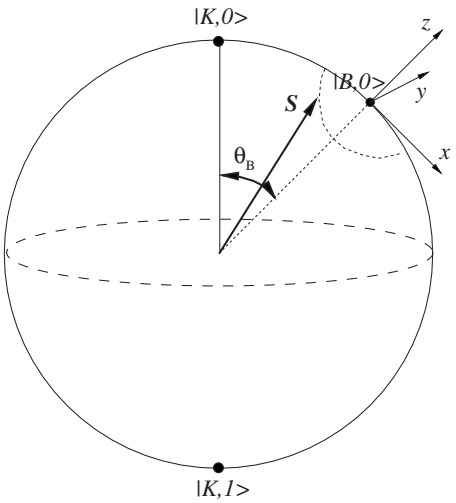

FIG. 9. Precession of the orbital pseudospin **S** around its equilibrium position with polar angle θ_B and azimuthal angle $\varphi_B=0$. This orientation is chosen as the orbital pseudospin quantization axis in the pseudospin wave model. The angle θ is the polar angle measured from the equilibrium orientation of the pseudospins.

$$|K,B,X\rangle = \cos\left(\frac{\theta_B}{2}\right)|K,0,X\rangle + \sin\left(\frac{\theta_B}{2}\right)|K,1,X\rangle, \quad (63)$$

where $\theta_B \in [0,\pi]$ has been defined in Eq. (50).

The collective mode corresponds to spatially coherent rotations of this spinor around its ground state value. For this reason, it is convenient to choose the orbital pseudospin quantization axis along the direction $|B,0\rangle$. In order to do this, we define 'bonding' and 'antibonding' electron creation operators by

$$b^\dagger_{B,K,X} = \cos\left(\frac{\theta_B}{2}\right)c^\dagger_{K,0,X} + \sin\left(\frac{\theta_B}{2}\right)c^\dagger_{K,1,X}, \quad (64)$$

$$b^\dagger_{AB,K,X} = \sin\left(\frac{\theta_B}{2}\right)c^\dagger_{K,0,X} - \cos\left(\frac{\theta_B}{2}\right)c^\dagger_{K,1,X}. \quad (65)$$

Below we use the convention that pseudospin up corresponds to state $|B,K\rangle$ and pseudospin down to state $|AB,K\rangle$ and we denote the pseudospin by $\mathbf{S}$.

In our GRPA system of equations for the collective modes, the orbital-pseudospin wave mode is decoupled from all other modes. Below we follow one possible strategy for explaining the physics of this mode by comparing our microscopic GRPA equation of motion to the equations of motion of an effective orbital pseudospin model, and using the comparison to identify the effective pseudospin interactions. Since collective modes correspond to small oscillations of the pseudospin around its quantization direction, we can use an effective model which has interactions only between transverse spins. (Quantization direction interactions can be represented as transverse interactions because of the spin-magnitude constraint.) We write the pseudospin effective Hamiltonian in momentum ($\mathbf{q}$) space:

$$H = N_\varphi \sum_{\mathbf{q}} J_{ij}(\mathbf{q})S_i(\mathbf{q})S_j(-\mathbf{q}), \quad (66)$$

where $i,j=x,y$. Since $J_{ij}(\mathbf{r},\mathbf{r}')$ in the real space version of Eq. (66) depends on $\mathbf{r}-\mathbf{r}'$ only, it follows that we can always write $J_{ij}(\mathbf{r})=J_{ji}(-\mathbf{r})$ and hence $J_{ij}(\mathbf{q})=J_{ji}(-\mathbf{q})$. Because the real-space interactions must be real we also have the usual property that $J_{ij}(\mathbf{q})=J^*_{ij}(-\mathbf{q})$. Combining these two identities we can conclude that $J_{xx}(\mathbf{q})$ and $J_{yy}(\mathbf{q})$ are real and even in $\mathbf{q}$, while $J_{xy}(\mathbf{q})$ has even real and odd imaginary contributions. The real parts of $J_{xy}(\mathbf{q})$ and $J_{yx}(\mathbf{q})$ are identical while their imaginary parts differ in sign. As we emphasize further below, the DM interaction is captured by the imaginary part of $J_{xy}(\mathbf{q})$.

The commutation relations between the spin operators when a projection to the lowest Landau level is made are $N_\varphi[S_i(\mathbf{q}),S_j(\mathbf{q}')]=i\varepsilon_{i,j,k}\cos(\mathbf{q}\times\mathbf{q}'\ell^2/2)S_k(\mathbf{q}+\mathbf{q}')$ for $i\neq j$ and $N_\varphi[S_i(\mathbf{q}),S_i(\mathbf{q}')]=-(i/2)\sin(\mathbf{q}\times\mathbf{q}'\ell^2/2)\rho(\mathbf{q}+\mathbf{q}')$ for $i=x,y$ where ρ is the total density. In a spin-wave approximation, we take the average value of the right-hand-sides of these expressions so that, in a liquid phase, we have the commuation relation

$$N_\varphi[S_x(\mathbf{q}),S_y(\mathbf{q}')] = \frac{1}{2}i\delta_{\mathbf{q},-\mathbf{q}'}, \quad (67)$$

the equations of motion of the pseudospin model are

$$\begin{pmatrix} -iJ_{xy}-\omega & -iJ_{yy} \\ iJ_{xx} & iJ_{yx}-\omega \end{pmatrix}\begin{pmatrix} S_x \\ S_y \end{pmatrix} = \begin{pmatrix} 0 \\ 0 \end{pmatrix} \quad (68)$$

with the dispersion relations

$$2\omega_\pm = -i(J_{xy}-J_{yx}) \pm \sqrt{4J_{xx}J_{yy}-(J_{xy}+J_{yx})^2}. \quad (69)$$

Note that the first term on the right hand side of Eq. (69) is real and odd in $\mathbf{q}$ and that it represents the contribution of the DM interaction to the collective mode frequency.

Comparing with our microscopic GRPA results for the equations of motion and collective mode frequencies, we obtain the following expressions for the pseudospin effective interactions:

$$J_{xx} = \frac{1}{2}A_3 + \Re[A_2] - \sin^2(\theta_B)\left(\frac{1}{2}A_1 + \Re[A_2]\right),$$

$$J_{yy} = \frac{1}{2}A_3 - \Re[A_2],$$

$$J_{xy} = -\frac{i}{2}\sin(\theta_B)A_4 - \cos(\theta_B)\Im[A_2],$$

$$J_{yx} = \frac{i}{2}\sin(\theta_B)A_4 - \cos(\theta_B)\Im[A_2], \quad (70)$$

with

$$A_1(q) = h_1(q) - x_1(q) + x_{16}(q) - h_{16}(q),$$

$$A_2(\mathbf{q}) = e^{2i\theta_\mathbf{q}}[\hat{h}_6(q) - \hat{x}_6(q)],$$

$$A_3(q) = 2h_1(q) - 2h_4(q) - 2x_4(q) + x_1(0),$$

$$A_4(\mathbf{q}) = -2\Re\{ie^{i\theta_\mathbf{q}}[\hat{h}_2(q) + \hat{h}_8(q) + \hat{x}_2(q) - \hat{x}_8(q)]\}, \quad (71)$$

where $\theta_\mathbf{q}$ is the angle between the wave vector $\mathbf{q}$ and the x axis. All interactions are defined in Appendix A. All Hartree and Fock interaction terms in Eqs. (71), $h_i,\hat{h}_i$ and $x_i,\hat{x}_i$, are real and depend only on the modulus of $\mathbf{q}$.

We see from the structure of Eqs. (70) that the dispersion relation has the symmetry $\omega_\pm(\Delta_B^{(2)}-\Delta_B)=\omega_\pm(\Delta_B)$. Because $\theta_B(\Delta_B^{(2)}-\Delta_B)=\pi-\theta_B(\Delta_B)$ [from Eq. (50)], it follows that the dispersion at small bias is the same as the dispersion near the critical bias as first pointed out in Ref. 12.

The physical content of the various terms in Eqs. (70) is most easily identified from their long-wavelength forms. From Eqs. (70) we find that at small q and small $\sin(\theta_B) \approx \theta_B \approx 2\sqrt{\Delta_B/\Delta_B^{(2)}}$,

$$J_{xx}(\mathbf{q}) \approx 2\beta\Delta_B + q\ell\cos^2(\theta_\mathbf{q}) + \frac{\sqrt{2\pi}}{32}q^2\ell^2[1-6\cos^2(\theta_\mathbf{q})], \quad (72)$$

$$J_{yy}(\mathbf{q}) \approx q\ell \sin^2(\theta_\mathbf{q}) - \frac{\sqrt{2\pi}}{32} q^2\ell^2[5 - 6\cos^2(\theta_\mathbf{q})], \quad (73)$$

$$J_{xy}(\mathbf{q}) \approx -\frac{1}{\sqrt{2}} i \sqrt{\sqrt{\frac{\pi}{2}}\beta\Delta_B q\ell \sin(\theta_\mathbf{q}) - q\ell \sin(\theta_\mathbf{q})\cos(\theta_\mathbf{q})}, \quad (74)$$

$$J_{yx}(\mathbf{q}) \approx \frac{1}{\sqrt{2}} i \sqrt{\sqrt{\frac{\pi}{2}}\beta\Delta_B q\ell \sin(\theta_\mathbf{q}) - q\ell \sin(\theta_\mathbf{q})\cos(\theta_\mathbf{q})}. \quad (75)$$

The pseudospin rotations which change S_x correspond to changes in the angle θ on the orbital pseudospin Bloch sphere relative to the ground state value θ_B as illustrated on Fig. 9. For this reason J_{xx} remains finite (is massive) as $q \to 0$ when the potential bias is finite unlike the other couplings. The terms proportional to $q\ell \cos^2(\theta_\mathbf{q})$ in J_{xx}, $q\ell \sin^2(\theta_\mathbf{q})$ in J_{yy} and $q\ell \sin(\theta_\mathbf{q})\cos(\theta_\mathbf{q})$ in J_{xy} and J_{yx} are simply electrostatic interactions between changes generated when the dipole orientation varies in space. (Recall that the charge density is equal to the divergence of the dipole density.) These terms are the long-wavelength limits of the Hartree interactions captured by the GRPA theory. The imaginary contribution to J_{xy} is the DM interaction whose physics we discuss below. The eigenvector for the pseudospin motion, at small q and small Δ_B, has $S_x/S_y = i\sqrt{2q\ell/\beta\Delta_B \sin(\theta_\mathbf{q})}$ if $\theta_\mathbf{q} \neq 0$ and $S_x/S_y = iq\ell\sqrt{2\pi/(16\beta\Delta_B)}$ if $\theta_\mathbf{q}=0$ so that the long wavelength collective modes are elliptical precessions with minor axis along the massive $\hat{x}$ direction and major axis along the $\hat{y}$ direction which contributes dipolar electrostatic energy. The long wavelength Goldstone collective mode energy therefore has unusual square root dispersion,

$$\omega(\mathbf{q}) = \sqrt{2\beta\Delta_B q\ell} \sin(\theta_\mathbf{q}). \quad (76)$$

For $\sin(\theta_\mathbf{q})=0$, we have the linear dispersion,

$$\omega(\mathbf{q}) = \frac{1}{4}\sqrt{\sqrt{2\pi}\beta\Delta_B} q\ell. \quad (77)$$

We see later that the DM interaction assumes a larger importance at larger bias potentials and shorter wavelengths.

The orbital coherent state occurs at finite bias and is preempted at small biases by the interlayer coherent state. It is nevertheless interesting to examine the artificial limit in which $\Delta_B \to 0$, but layer degrees of freedom are still not in play. In that limit all electrons would be in the $n=0$ orbital, there would be no electric dipoles in the ground state, and the exchange parameters would be given by

$$J_{xx} = \frac{1}{2}A_3 + \Re[A_2],$$

$$J_{yy} = \frac{1}{2}A_3 - \Re[A_2],$$

$$J_{xy} = -\Im[A_2],$$

$$J_{yx} = -\Im[A_2]. \quad (78)$$

The dispersion relation would then be given by

$$\omega(q) = \frac{1}{2}\sqrt{A_3^2(q) - 4|A_2(\mathbf{q})|^2}, \quad (79)$$

which is isotropic. The long-wavelength limit dispersion would become

$$\omega_\pm(q) \approx \frac{1}{4}\left(\frac{\pi}{2}\right)^{1/4} (q\ell)^{3/2}, \quad (80)$$

similar to $\nu=-3$ behavior.[7]

C. Moriya interaction and spiral state instability

As explained previously the DM interaction is captured by the imaginary part of $J_{xy}(\mathbf{q})$. When this contribution to the orbital pseudospin Hamiltonian is isolated it yields an interaction of the standard[15] DM form,

$$H_{DM} = iN_\varphi \sum_\mathbf{q} \Im[J_{xy}(\mathbf{q})][\mathbf{S}(\mathbf{q}) \times \mathbf{S}(-\mathbf{q})] \cdot \hat{\mathbf{z}}. \quad (81)$$

An examination of Eqs. (71) shows that this interaction is not due to electrostatic dipole interactions, and instead to the exchange vertex corrections i.e., to the interactions $x_2(q)$ and $x_8(q)$. In Appendix C, we analyze the exchange energy of quantum Hall ferromagnets quite generally and show that DM interactions are the rule rather than the exception when the two states from which the pseudospin is constructed have the same spin. The physics of exchange interaction contributions to collective mode energies is most simply described by making a particle-hole transformation for occupied states, as discussed in Appendix C. The exchange interaction at momentum p can then be related[18] to the attractive interaction between an electron and a hole separated by $p\ell^2$. DM interactions occur when the pseudospin state of the electron or hole give rise to cyclotron orbit charge distributions which do not have inversion symmetry, a property that holds here because of dipole formation. These distortions of the cyclotron orbit are irrelevant when p is very large but become important for $p \sim \ell^{-1}$. In the case of a simple parabolic band $\nu=1$ quantum Hall ferromagnet, for example, this picture[18] provides a simple understanding of the full spin-wave dispersion.

The DM interaction is strongest at $\Delta_B/\Delta_B^{(2)}=1/2$, i.e., when $\sin(\theta_B)=1$. We have found that over a broad range of Δ_B values the DM interaction is strong enough to induce an instability of the uniform coherent state. When viewed as a classical complex-variable quadratic form for Gaussian energy fluctuations, the orbital pseudospin Hamiltonian, Eq. (66), is positive definite provided that $J_{xx}(\mathbf{q})$ is positive, $J_{yy}(\mathbf{q})$ is positive, and

$$J_{xx}(\mathbf{q})J_{yy}(\mathbf{q}) > |J_{xy}(\mathbf{q})|^2. \quad (82)$$

Explicit numerical calculations show that the first two stability requirements are always satisfied, but that because of the DM interaction, the third is not satisfied when $\sin(\theta_B)$ is large. In the GRPA we find that the OPM first becomes soft

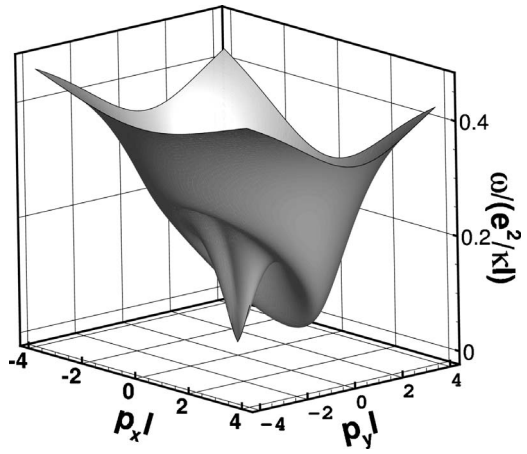

FIG. 10. Dispersion relation in the orbital-coherent state at the Dzyaloshinskii-Moriya instability. Filling factor $\nu=-1$ and bias $\Delta_B=0.51\ e^2/\kappa\ell$.

at $q_y\ell\approx 2$ when $\Delta_B=\Delta_B^{(DM)}\approx\Delta_B^{(2)}/10$. (We have $\theta_B\approx 41°$ at this value of Δ_B.) Fig. 10 shows the instability of the orbital-pseudospin mode at $\Delta_B^{(DM)}$. We remark that the instability occurs at a positive (negative) value of q_y in $\omega_+(\omega_-)$. The higher-energy collective modes (not shown in the figure) show no sign of instability.

The eigenvector with positive frequency of Eq. (68) has

$$\frac{S_x}{S_y}=\frac{-J_{xy}-J_{yx}+i\sqrt{4J_{xx}J_{yy}-(J_{xy}+J_{yx})^2}}{2J_{xx}}. \tag{83}$$

It follows, using Eq. (82), that, at the DM instability, the energy is lowered by forming coupled density-waves in $\hat{x}$ and $\hat{y}$ pseudospin components with

$$\frac{S_x(\mathbf{q})}{S_y(\mathbf{q})}=-\frac{J_{xy}(\mathbf{q})}{J_{xx}(\mathbf{q})}=-\frac{J_{yy}(\mathbf{q})}{J_{xy}^*(\mathbf{q})}. \tag{84}$$

The real part of the J_{xy} coupling, due mainly to the dipole electrostatic energy, is very small at the instability wave vector because the $N=0$ Landau level cannot support rapid spatial variation, as we have verified by explicit calculation. Because $J_{yy}(\mathbf{q})$ is real, it follows that S_x and S_y spatial variations are out of phase by nearly exactly $\pi/2$. If the magnitudes of the S_x and S_y components were identical, this would imply a spiral ground state. Because $J_{xx}(\mathbf{q})$ and $J_{yy}(\mathbf{q})$ are not identical at the instability, the spiral is somewhat distorted. It must be kept in mind, however, that the DM instability may be preempted by a first order transition to a state with lower energy and a more complex pseudospin pattern. A fuller exploration of the properties of these states, including their properties in the presence of an external electric field, is beyond the scope of the present work.

IX. COLLECTIVE MODES IN THE MIXED STATE

The mixed state occurs between the interlayer coherent and interorbital coherent phases as shown in Fig. 3. The width of this region in the phase diagram increases with magnetic field. In this phase, all order parameters are finite so that this phase has both interlayer and interorbital coherence. We show the behavior of some of these order parameters with bias in Fig. 4. The order parameters $\langle\rho_{0,1}^{K,K'}\rangle$ and $\langle\rho_{1,0}^{K,K'}\rangle$ which flip both valley and orbital indices are nonzero in this phase.

The collective modes in the MS are obtained numerically by solving Eq. (34). The MS has three dispersive modes, as in the other two phases we studied. The dispersions of these modes differ from the dispersions in the other two phases at small wave vector only. The interorbital pseudospin mode is gapless and does not show up in the absorption spectrum. For the interlayer pseudospin mode, we find an instability for $q<q_c$ where $q_c\ell\sim 0.00012$. But, the mixed state is difficult to stabilize numerically so that it is difficult to say if this instability is genuine or due to the fact that we did not find the precise (complex) order parameters. If the phase is stable, then the inter-layer pseudospin mode is also gapless and does not show up in the absorption. If it is not stable, the ground state is probably a modulated state. As we discussed in the last section, the mixed state disappears if corrections to our model are introduced so that we do not discuss it further in this paper.

X. MICROWAVE ABSORPTION

The collective modes discussed in the previous sections can be detected in microwave absorption experiments, as we now show. We write the current operator, projected onto $N=0$ and valley K, as

$$j_{\xi K,i}=-c\left.\frac{\partial H_{\xi K}^0}{\partial A_i^e}\right|_{A_i^e=0}, \tag{85}$$

where A_i^e is the vector potential of the external electromagnetic field, $i=x,y$ and H_K^0 is given in Eq. (2). In second quantization, the total current is given by

$$\mathbf{J}_{\xi K}=\int d\mathbf{r}\Psi_{\xi K}^\dagger(\mathbf{r})\mathbf{j}_{\xi K}\Psi_{\xi K}(\mathbf{r}), \tag{86}$$

with the field operators defined in Eqs. (7) and (8) and $\xi=\pm 1$. We find that

$$\mathbf{J}_{\xi K}=\xi\sqrt{2}\beta\Delta_B\frac{e\ell}{\hbar}N_\varphi(\rho_{\xi K,y}(0)\hat{\mathbf{x}}+\rho_{\xi K,x}(0)\hat{\mathbf{y}}), \tag{87}$$

where

$$\rho_{K,x}(0)=\frac{1}{2}[\rho_{0,1}^{K,K}(0)+\rho_{1,0}^{K,K}(0)], \tag{88}$$

$$\rho_{K,y}(0)=\frac{1}{2i}[\rho_{0,1}^{K,K}(0)-\rho_{1,0}^{K,K}(0)], \tag{89}$$

and similarly for $\rho_{K',x/y}(0)$. The same result for $\mathbf{J}_{\xi K}$ can be obtained by calculating the polarization current

$$\mathbf{J}_{\xi K}=\frac{d}{dt}\mathbf{d}_{\xi K}(\mathbf{q}), \tag{90}$$

with the dipole density $\mathbf{d}_{\xi K}(\mathbf{q})$ defined in Eq. (62) and using the Heisenberg equation of motion $-i\hbar d/dt(\ldots)$

$=[H^0_{\xi K},(\ldots)]$. We note that the orbitally coherent state has spontaneous currents in its ground state, a very exceptional property. It appears likely that, in finite systems, these currents should flow perpendicular to system boundaries, forcing domain structures in the pseudospin magnetization texture, consistent with expectations based on the electrostatic energy of the dipole density.

We define the total current-current correlation function Matsubara Green's functions as

$$\chi_{J_\alpha J_\beta}(\tau) = -\frac{1}{S}\langle T J_\alpha(\tau) J_\beta(0)\rangle = \left(\frac{\Delta_B}{\gamma_1}\right)^2 \frac{e^2\hbar^2}{4\pi m^{*2}\ell^4} \sum_{i,j=K,K'} \xi_i\xi_j \chi_{\rho_{i,\bar{\alpha}},\rho_{j,\bar{\beta}}}(\tau), \quad (91)$$

where $J_\alpha = J_{K,\alpha} + J_{K',\alpha}$ and

$$\chi_{\rho_{i,\alpha},\rho_{j,\beta}}(\tau) = -\langle T\rho_{i,\alpha}(0,\tau)\rho_{j,\beta}(0,0)\rangle. \quad (92)$$

with $i,j=K,K'$ and $\alpha,\beta=x,y$. Note that $\bar{\alpha},\bar{\beta}$ are defined so that $\bar{x}=y$, $\bar{y}=x$.

The microwave absorption for an electric field oriented along the direction α is given by

$$P_\alpha(\omega) = -\frac{1}{\hbar}\Im\left[\frac{\chi^R_{J_\alpha J_\alpha}(\omega)}{\omega+i\delta}\right]E_0^2 = -\frac{1}{2}\left(\frac{e^2}{h}\right)\left(\frac{\Delta_B}{\gamma_1}\right)^2 \omega_c^{*2} \sum_{i,j=K,K'} \Im\left[\xi_i\xi_j \frac{\chi^R_{\rho_{i,\bar{\alpha}},j,\bar{\alpha}}(\omega)}{\omega+i\delta}\right]E_0^2, \quad (93)$$

where we have assumed a uniform electric field $\mathbf{E}(t) = E_0\hat{\alpha}e^{-i\omega t}$ and taken the analytic continuation $i\Omega_n \to \omega + i\delta$ of $\chi_{J_\alpha J_\alpha}(0,\Omega_n)$ to get the retarded response function. The response functions $\chi^R_{\rho_{i\alpha}\rho_{j\alpha}}$ are calculated in units of $\hbar/(e^2/\kappa\ell)$ so that $P_\alpha(\omega)$ is the power absorbed per unit area. In Eq. (93) we have neglected a diamagnetic contribution to the current response which becomes important at low frequencies.

Our GRPA correlation functions are given by Eq. (34) and numerical results for the absorption in the interlayer coherent phase are shown in Fig. 11. Exactly the same result is obtained, in this phase, if the electric field is set in the y direction, i.e., the absorption is isotropic. We see that the signal in the absorption is at a frequency corresponding to the orbital-pseudospin mode (see Fig. 6). The frequency ν of this mode at $\mathbf{q}=0$ decreases with bias (see Fig. 12) while the absorption intensity increases with bias. Since $e^2/\hbar\kappa\ell \sim 2.7 \times 10^3\sqrt{B(\mathrm{T})}$ GHz (using $\kappa=5$ for graphene on SiO_2 substrate), the frequency of the orbital pseudospin mode at zero bias is $\nu \approx 3.4$ GHz, i.e., in the microwave regime. Note that mode 3 in Fig. 5 is also present in the absorption at finite bias and that its frequency has a higher value outside of the microwave regime. Our current calculation does not take into consideration the coupling with disorder or with other excitations that could degrade these collective modes. We thus have no information on the linewidth of these modes.

In the orbital-coherent phase, the orbital-pseudospin mode is gapless and decoupled from the two other gapped modes.

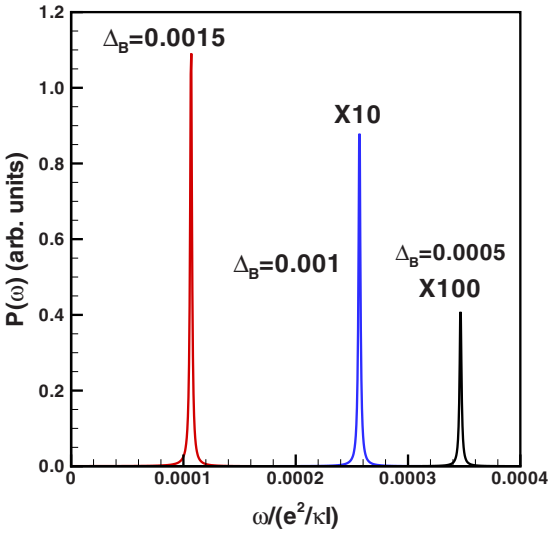

FIG. 11. (Color online) Microwave absorption from the orbital pseudospin mode in the interlayer phase at different values of the bias. The absorption is zero at zero bias. The second (third) peak has been multiplied by 10(100).

Since the orbital-coherent mode couples strongly to external electric fields, we can expect anomalous low-frequency absorption in this state, similar to the Drude absorption of a metal. This interesting and unusual absorption feature is likely to be highly sensitive to disorder. Its detailed analysis lies beyond the scope of the present paper. Above $\Delta_B^{(2)}$, the ground state has $\nu_{K,1}=\nu_{K',0}=\nu_{K',1}=1$ and there is no orbital coherence anymore. The OPM then has a gap that is proportional to $\Delta_B - \Delta_B^{(2)}$. The OPM becomes visible in the absorption in this phase while the other modes do not.

In summary, we see that the interlayer and interorbital coherent phases in the phase diagram at $\nu=-1$ have a differ-

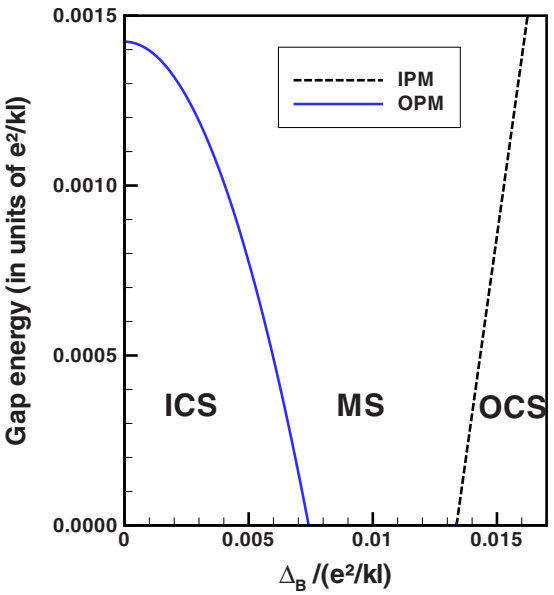

FIG. 12. (Color online) Gaps in the inter-layer pseudospin mode (IPM) and in the orbital pseudospin mode (OPM) as a function of bias at $\nu=-1$ and $B=40$ T. In the mixed state, both gaps are zero if the state is stable.

ent signature in the microwave absorption spectrum.

XI. DISCUSSION

We have studied the phase diagram and collective excitations of a spin-polarized bilayer graphene 2DEG at filling factors $\nu=-1$ and $\nu=3$, as a function of a bias electric potential which shifts electrons between layers. Our study is based on the Hartree-Fock approximation for the mean-field ground state and the GRPA for the collective modes and response functions.

We predict phase transitions between the following sequence of states with increasing potential bias: (1) an interlayer-coherent state (ICS) with a zero gap inter-layer pseudospin mode (IPM) and an orbital pseudospin mode (OPM) with a small gap. This gap can be detected in microwave absorption experiment. Its frequency decreases with bias while its intensity increases with bias; (2) a mixed state (MS) with both interlayer and interorbital coherence. Both the IPM and OPM are gapped and visible in microwaves in this phase. Moreover, the intensity of the absorption is highly sensitive to the direction of the external electric field; (3) an orbital coherent state (OCS) with orbital coherence concentrated in one layer only. (The second layer is completely filled.) The OCS state is a very simple one in which the low potential layer is filled and the high potential layer has a gap induced between it's two Landau levels by spontaneously establishing coherence between states with $n=1$ and $n=0$ orbital character. This state has a number of quite unusual properties, including electric dipoles and associated uniform currents in its ground state. The OCS has a gapless (Goldstone) OPM and a gapped IPM. Both modes are absent from the absorption spectrum. The dispersions of the collective modes are also highly anisotropic in this phase. The phase is unstable at a finite wave vector due to the presence of a Dzyaloshinksii-Moriya exchange interaction. We believe that the instability will lead to the formation of a ground state with a non-uniform pseudosopin pattern.

The properties of the orbital state are associated with a competition between an electron-electron interaction term which favors $n=0$ orbital occupation, and single-particle terms in the effective two-band model of Ref. 5 which favors $n=1$ orbital occupation more strongly at larger interlayer potential difference. Strictly speaking, our phase diagram is valid within the range of validity of the simplified two-band model of Ref. 5 used for the electronic band structure of bilayer graphene. In this model, the warping term γ_3 is neglected as well as the γ_4 hopping term which connects sites $A_1(B_1)$ and $A_2(B_2)$ and the term Δ which is the difference in the crystal field experienced by the inequivalent carbon atoms A and B that are part of a dimer. Because the correction $\beta\Delta_B$ in Eqs. (3) and (6) is very small, we have to consider the effect of the neglected terms γ_4 and Δ. In the two-band model, we find (see Ref. 19, for example)

$$E_{\xi K,n=0,X}=\frac{1}{2}\xi\Delta_B, \tag{94}$$

$$E_{\xi K,n=1,X}=\frac{1}{2}\xi\Delta_B-\beta\xi\Delta_B+\zeta, \tag{95}$$

where ζ is independent of the bias Δ_B and of the valley index and is given by

$$\zeta=2\beta\left(\frac{\gamma_4}{\gamma_0}\right)\gamma_1+\beta\left(1+\frac{\gamma_4^2}{\gamma_0^2}\right)\Delta. \tag{96}$$

The correction ζ lifts the degeneracy of the $n=0,1$ states at zero bias. Because γ_4 and Δ are both positive,[22] this correction moves the energy of the state $n=0$ below that of the state $n=1$ in *both* valleys at small bias. The values of γ_4 and Δ are not precisely known. Recent measurements give $\gamma_4/\gamma_0=0.04-0.07$ and $\Delta/\gamma_0=0.005-0.008$ in graphene bilayer (see Table I in Ref. 20 and references given therein). Because ζ acts effectively as a finite bias of the order of 3 meV at $B=10$ T, it has the effect of suppressing the mixed state and pushing the onset of the orbital state to higher bias without modifying significantly its range of existence.[21] The intermediate phase between the inter-layer coherent state and the orbital state is a new polarized state with $\nu_{K,0}=\nu_{K',0}=\nu_{K',1}=1$.

If spin is included in our model, we have to worry that at large bias, the spin up states in the top layer will mix with the spin down states in the K' layer at $\nu=-1$. This mixed spin state may then compete with the interorbital state. The full Hartree-Fock phase diagram for the $N=0$ octet in the presence of a bias will be discussed elsewhere.[21] We remark, however, that the orbital state will still be accessible at $\nu=+3$ where no spin mixing is expected for states in the K (top) layer.

Even with the neglect of γ_4, Δ and spin corrections, the interlayer and mixed states may be difficult to observe experimentally. As we discussed in Sec. VII, the small value of the radio d/ℓ causes the transition to the mixed state to occur at very small value of the bias Δ_B of the order of 0.3 meV for graphene on a SiO_2 substrate. We may expect the interlayer and mixed state to be fragile with respect to disorder and other symmetry breaking terms that are beyond our Hartree-Fock approximation and continuum model. Moreover the small orbital pseudospin order in the mixed phase may also be destroyed by quantum fluctuations. The interorbital state, however, survives to much higher values of the bias, of the order of 900 meV,[26] and should be accessible experimentally. We note however that spin degrees of freedom are more likely to play a role at larger bias voltages. Although we have not explicitly accounted for spin degrees of freedom in this paper, we anticipate that unusual ordered states can still occur at odd integer filling factors even when the spin degree of freedom is active.

ACKNOWLEDGMENTS

A.-H.M. was supported by the NSF under Grant No. DMR-0606489 and by the Welch Foundation. R.C. was supported by a grant from the Natural Sciences and Engineering Research Council of Canada (NSERC). Y.B. was supported by a grant from the State of Florida. Computer time was

provided by the Réseau Québécois de Calcul Haute Performance (RQCHP).

APPENDIX A: HARTREE AND FOCK INTERACTIONS

We first give the definitions of the Hartree, H, and Fock, X, interactions in Eqs. (12)–(15),

$$h_1(q) = H_{0,0,0,0}(q) = \frac{1}{q\ell}\Lambda(q), \tag{A1}$$

$$h_2(\mathbf{q}) = H_{0,0,0,1}(\mathbf{q}) = -\frac{i}{\sqrt{2}}e^{i\theta_\mathbf{q}}\Lambda(q), \tag{A2}$$

$$h_4(q) = H_{0,0,1,1}(q) = \frac{1}{q\ell}\left(1 - \frac{q^2\ell^2}{2}\right)\Lambda(q), \tag{A3}$$

$$h_6(\mathbf{q}) = H_{0,1,0,1}(\mathbf{q}) = \frac{1}{2}q\ell e^{2i\theta_\mathbf{q}}\Lambda(q), \tag{A4}$$

$$h_7(q) = H_{0,1,1,0}(q) = \frac{1}{2}q\ell\Lambda(q), \tag{A5}$$

$$h_8(\mathbf{q}) = H_{0,1,1,1}(\mathbf{q}) = \frac{i}{\sqrt{2}}e^{i\theta_\mathbf{q}} \times \left(1 - \frac{q^2\ell^2}{2}\right)\Lambda(q), \tag{A6}$$

$$h_{16}(q) = H_{1,1,1,1}(q) = \frac{1}{q\ell}\left(1 - \frac{q^2\ell^2}{2}\right)\Lambda(q) \tag{A7}$$

and

$$h_3 = H_{0,0,1,0}(\mathbf{q}) = -h_2^*, \tag{A8}$$

$$h_5 = H_{0,1,0,0}(\mathbf{q}) = -h_2, \tag{A9}$$

$$h_9 = H_{1,0,0,0}(\mathbf{q}) = h_2^*, \tag{A10}$$

$$h_{10} = H_{1,0,0,1}(q) = h_7, \tag{A11}$$

$$h_{11} = H_{1,0,1,0}(\mathbf{q}) = h_6^*, \tag{A12}$$

$$h_{12} = H_{1,0,1,1}(\mathbf{q}) = -h_8^*, \tag{A13}$$

$$h_{13} = H_{1,1,0,0}(q) = h_4, \tag{A14}$$

$$h_{14} = H_{1,1,0,1}(\mathbf{q}) = -h_8, \tag{A15}$$

$$h_{15} = H_{1,1,1,0}(\mathbf{q}) = h_8^*, \tag{A16}$$

where $\theta_\mathbf{q}$ is the angle between the wave vector $\mathbf{q}$ and the x axis and $\Lambda(q)=\exp(\frac{-q^2\ell^2}{2})$. The interactions $\tilde{h}_n(\mathbf{q})$ are obtained by multiplying h_n by e^{-qd} where d is the interlayer separation. The interactions $\hat{h}_n(\mathbf{q})$ and $\hat{\tilde{h}}_n$ are obtained by removing the term i and the phase factor $e^{\pm i\theta_\mathbf{q}}$ or $e^{\pm 2i\theta_\mathbf{q}}$ in h_n and $\tilde{h}_n$. For example $\hat{h}_2=-\Lambda(q)/\sqrt{2}$ while $h_2(\mathbf{q})=-\frac{i}{\sqrt{2}}e^{i\theta_\mathbf{q}}\Lambda(q)$.

The Fock interactions are defined by

$$x_1(q) = X_{0,0,0,0}(\mathbf{q}) = \int_0^\infty dy e^{-y^2/2}J_0(q\ell y), \tag{A17}$$

$$x_2(\mathbf{q}) = X_{0,0,0,1}(\mathbf{q}) = \frac{i}{\sqrt{2}}e^{i\theta_\mathbf{q}}\int_0^\infty dyy e^{-y^2/2}J_1(q\ell y), \tag{A18}$$

$$x_4(q) = X_{0,0,1,1}(\mathbf{q}) = \int_0^\infty dy\left(1 - \frac{y^2}{2}\right)e^{-y^2/2}J_0(q\ell y), \tag{A19}$$

$$x_6(\mathbf{q}) = X_{0,1,0,1}(\mathbf{q}) = \frac{1}{2}e^{2i\theta_\mathbf{q}}\int_0^\infty dyy^2 e^{-y^2/2}J_2(q\ell y), \tag{A20}$$

$$x_7(q) = X_{0,1,1,0}(\mathbf{q}) = \frac{1}{2}\int_0^\infty dyy^2 e^{-y^2/2}J_0(q\ell y), \tag{A21}$$

$$x_8(\mathbf{q}) = X_{0,1,1,1}(\mathbf{q}) = -\frac{i}{\sqrt{2}}e^{i\theta_\mathbf{q}}\int_0^\infty dyy \times\left(1 - \frac{y^2}{2}\right)e^{-y^2/2}J_1(q\ell y), \tag{A22}$$

$$x_{16}(q) = X_{1,1,1,1}(\mathbf{q}) = \int_0^\infty dy\left(1 - \frac{y^2}{2}\right)^2 e^{-y^2/2}J_0(q\ell y), \tag{A23}$$

and

$$x_3 = X_{0,0,1,0}(\mathbf{q}) = x_2^*, \tag{A24}$$

$$x_5 = X_{0,1,0,0}(\mathbf{q}) = -x_{2,} \tag{A25}$$

$$x_9 = X_{1,0,0,0}(\mathbf{q}) = -x_2^*, \tag{A26}$$

$$x_{10} = X_{1,0,0,1}(q) = x_7, \tag{A27}$$

$$x_{11} = X_{1,0,1,0}(\mathbf{q}) = x_6^*, \tag{A28}$$

$$x_{12} = X_{1,0,1,1}(\mathbf{q}) = x_8^*, \tag{A29}$$

$$x_{13} = X_{1,1,0,0}(q) = x_4, \tag{A30}$$

$$x_{14} = X_{1,1,0,1}(\mathbf{q}) = -x_8, \tag{A31}$$

$$x_{15} = X_{1,1,1,0}(\mathbf{q}) = -x_8^*. \tag{A32}$$

The interactions $\tilde{x}_n$ are obtained by multiplying the integrand by $e^{-yd/\ell}$. The interactions $\hat{x}_n$ and $\hat{\tilde{x}}_n$ are obtained by removing the imaginary term i and the phase factor.

The combinations

$$H_i = h_i - \tilde{h}_i, \tag{A33}$$

$$T_i = h_i + \tilde{h}_i, \tag{A34}$$

$$X_i = x_i + \tilde{x}_i, \tag{A35}$$

$$U_i = x_i - \tilde{x}_i. \tag{A36}$$

To define $\hat{H}_n, \hat{T}_n, \hat{X}_n, \hat{U}_n$, we follow the same procedure as for $\hat{h}_n, \hat{\tilde{h}}_n, \hat{x}_n, \hat{\tilde{x}}_n$.

Some useful constants,

$$x_1(0) = \sqrt{\frac{\pi}{2}}, \tag{A37}$$

$$x_4(0) = \frac{1}{2}\sqrt{\frac{\pi}{2}}, \tag{A38}$$

$$x_7(0) = \frac{1}{2}\sqrt{\frac{\pi}{2}}, \tag{A39}$$

$$x_{16}(0) = \frac{3}{4}\sqrt{\frac{\pi}{2}}. \tag{A40}$$

APPENDIX B: MATRIX F_1 FOR THE INTER-LAYER-COHERENT MODES

The density-matrix equations of motions which describe the three $\nu=-1$ spin-diagonal dispersive collective modes are usually simplest when written in the basis of the bonding and antibonding single-particle Hartree-Fock eigenstates. For the interlayer coherent state (ICS) (which is the ground state for $\Delta_B < \Delta^{(3)}_{B,num}$) we find that,

$$(I(\omega + i\delta) - F_1)\begin{pmatrix} ie^{-i\theta_{\mathbf{q}}}\rho_{AB1,B0} \\ ie^{i\theta_{\mathbf{q}}}\rho_{B0,AB1} \\ \rho_{AB1,B1} \\ \rho_{B1,AB1} \\ ie^{i\theta_{\mathbf{q}}}\rho_{AB0,AB1} \\ ie^{-i\theta_{\mathbf{q}}}\rho_{AB1,AB0} \end{pmatrix} = \begin{pmatrix} 0 \\ 0 \\ 0 \\ 0 \\ 0 \\ 0 \end{pmatrix}, \tag{B1}$$

where $\theta_{\mathbf{q}}$ is the angle between the two-dimensional wave vector $\mathbf{q}$ and the x axis, and B and AB refer to the states

$$|B,n,X\rangle = g_-|K,n,X\rangle + g_+|K',n,X\rangle, \tag{B2}$$

$$|AB,n,X\rangle = g_+|K,n,X\rangle - g_-|K',n,X\rangle, \tag{B3}$$

where $n=0,1$,

$$g_\pm = \sqrt{\frac{1 \pm \sigma}{2}}, \tag{B4}$$

and

$$\sigma = \frac{\Delta_B}{\Delta_B^{(1)}}. \tag{B5}$$

The matrix F_1 depends only on the modulus of the wave vector $\mathbf{q}$ so that the dispersions are isotropic. This matrix is given by

$$F_1(q) = \frac{1}{2}\begin{pmatrix} -A-\sigma^2 B & fH & -N+\sigma^2 J & -fJ & \sigma\sqrt{f}H & -\sigma\sqrt{f}G \\ -fH & A+\sigma^2 B & fJ & N-\sigma^2 J & \sigma\sqrt{f}G & -\sigma\sqrt{f}H \\ -N+\sigma^2 J & -fJ & -C-\sigma^2 D & fM & -\sigma\sqrt{f}J & -\sigma\sqrt{f}J \\ fJ & N-\sigma^2 J & -fM & C+\sigma^2 D & \sigma\sqrt{f}J & \sigma\sqrt{f}J \\ -\sigma\sqrt{f}H & \sigma\sqrt{f}G & \sigma\sqrt{f}J & \sigma\sqrt{f}J & -E-\sigma^2 F & K-\sigma^2 H \\ -\sigma\sqrt{f}G & \sigma\sqrt{f}H & -\sigma\sqrt{f}J & -\sigma\sqrt{f}J & -K+\sigma^2 H & E+\sigma^2 F \end{pmatrix}, \tag{B6}$$

where

$$f = 1 - \sigma^2 \tag{B7}$$

The elements of the matrix $F_1(q)$ are defined by

$$A(q) = \tilde{x}_4(0) - \tilde{x}_1(0) - \frac{3}{4}x_1(0) - \tilde{x}_{16}(0) + X_4(q) - H_1(q) + H_4(q), \tag{B8}$$

$$B(q) = 2\Delta_B^c(\beta - 1) + H_1(q) - H_4(q) - U_4(q) + \tilde{x}_1(0) - \frac{5}{4}x_1(0) - \tilde{x}_4(0) + \tilde{x}_{16}(0) + 2\frac{d}{\ell}, \tag{B9}$$

$$C(q) = -H_{16}(q) + X_{16}(q) - 2\tilde{x}_{16}(0), \tag{B10}$$

$$D(q) = 2\Delta_B^c(2\beta - 1) + H_{16}(q) - U_{16}(q) + 2\tilde{x}_{16}(0) - \frac{3}{2}x_1(0) + 2\frac{d}{\ell}, \tag{B11}$$

$$E(q) = T_4(q) + X_4(q) - T_1(q) + \tilde{x}_1(0) - \tilde{x}_4(0) - \frac{3}{4}x_1(0) - \tilde{x}_{16}(0), \tag{B12}$$

$$F(q) = 2\beta\Delta_B^c - H_1(q) + H_4(q) + U_4(q) + \tilde{x}_4(0) - \tilde{x}_1(0) - \frac{1}{4}x_1(0) + \tilde{x}_{16}(0), \tag{B13}$$

$$G(q) = \Delta_B^c - H_1(q) + H_4(q) + U_4(q) + \tilde{x}_4(0) - \tilde{x}_1(0) + \frac{1}{2}x_1(0) - \frac{d}{\ell}, \tag{B14}$$

$$H(q) = \hat{H}_6(q) - \hat{U}_6(q), \tag{B15}$$

$$J(q) = \hat{H}_8(q) - \hat{U}_8(q), \tag{B16}$$

$$K(q) = \hat{X}_6(q) - \hat{T}_6(q), \tag{B17}$$

$$M(q) = H_{16}(q) - U_{16}(q), \tag{B18}$$

$$N(q) = \hat{H}_8(q) - \hat{X}_8(q). \tag{B19}$$

From Eq. (B6), it is easy to see that the dispersion of the OPM at zero bias (given by the 2×2 block in the lower right of the matrix F_1) is given by

$$\omega_{OPM}(\mathbf{q}) = \frac{1}{2}\sqrt{E^2(\mathbf{q}) - K^2(\mathbf{q})}, \tag{B20}$$

At $q=0$, we have

$$|E(0)| = \left| -\frac{1}{4}\sqrt{\frac{\pi}{2}} + \tilde{x}_1(0) - \tilde{x}_{16}(0) \right| = x_1(0) - \tilde{x}_1(0) - x_{16}(0) + \tilde{x}_{16}(0), \tag{B21}$$

$$K(0) = 0. \tag{B22}$$

APPENDIX C: EXCHANGE ENERGY PSEUDOSPIN DEPENDENCE

It is possible to derive a rather general and instructive expression for the exchange energy of a pseudospin-1/2 quantum Hall ferromagnet, for the case in which the pseudospin texture varies in one direction only. In the following we take this direction to be the $\hat{x}$ direction and choose a Landau gauge in which the guiding centers orbits are localized as a function of this coordinate. If we are interested only in the dependence of energy on pseudospin texture we can assume that every guiding center orbital is occupied by one electron, but leave the pseudospin of that orbital arbitrary. It is not necessary to immediately specify the orbital character of the states that form the pseudospin and we refer to them for the moment as state A and state B. In the case of immediate interest in this paper, state A has $n=0$ orbital character and state B has $n=1$ orbital character. We discuss some other examples below.

The pseudospin texture can be specified by the two-component pseudospinors at each guiding center,

$$|\Psi_X\rangle = \begin{pmatrix} z_X^A \\ z_X^B \end{pmatrix}, \tag{C1}$$

or by the guiding center dependent direction cosines of the pseudospin orientation: $(n_X^x, n_X^y, n_X^z) = [\sin(\theta_X)\cos(\phi_X), \sin(\theta_X)\sin(\phi_X), \cos(\theta_X)]$ where θ_X and ϕ_X are the pseudospin orientation polar and azimuthal angles. When a specific gauge choice is convenient we use $z^A = \cos(\theta/2)$ and $z^B = \sin(\theta/2)\exp(i\phi)$.

The exchange energy of a pseudospin quantum Hall ferromagnet is

$$E_x = -\frac{1}{2}\sum_{X,X'} \langle X, X'|V_{ee}|X', X\rangle. \tag{C2}$$

The dependence of exchange energy on pseudospin texture can be exhibited explicitly by using the property that each $\exp[i\mathbf{k}\cdot(\mathbf{r_1}-\mathbf{r_2})]$ term in the Fourier expansion of the two-particle interaction matrix elements can be separated into factors that depend on $\mathbf{r}_1$ and $\mathbf{r}_2$ independently. It follows that

$$E_x = -\frac{1}{2}\sum_{X,X'} n_{X'}^{\alpha} J_{X',X}^{\alpha,\beta} n_X^{\beta} \tag{C3}$$

where the Greek indices $\alpha = c, x, y, z$, $n^c \equiv 1$ represents the filling factor of the guiding center states,

$$J_{X',X}^{\alpha,\beta} = \frac{1}{A}\sum_{\mathbf{q}} \exp(-q^2\ell^2/2) f^{\alpha,\beta}(\mathbf{q}) V(\mathbf{q}) \delta_{X'-X,\ell^2 q_y}, \tag{C4}$$

ℓ is the magnetic length, $V(\mathbf{q})$ is the Fourier-transform of the electron-electron interaction and $f^{\alpha,\beta}(\mathbf{q})$ is an interaction form factor. Equation (C4) follows from the following expression for the plane-wave matrix elements,

$$\langle X'|\exp(i\mathbf{q}\cdot\mathbf{r})|X\rangle = \delta_{X',X+\ell^2 q_y} \exp(-q^2\ell^2/4) \times \sum_{I',I} \bar{z}_{X'}^{I'} F^{I',I}(\mathbf{q}) z_X^I, \tag{C5}$$

where the overbar accent denotes complex conjugation. The character of the cyclotron orbitals in the two nearly degenerate Landau levels is captured by the single-particle form factors $F^{I',I}(\mathbf{q})$. For example if pseudospin I has orbital Landau-level index n_I, $F^{I',I}(\mathbf{q}) = F_{n_{I'},n_I}(\mathbf{q})$ where $F_{n',n}(\mathbf{q})$ is the familiar two-dimensional electron gas Landau-level form factor,[25] commonly used in the analysis of many-different properties in the quantum Hall regime. Note that $F^{I',I}(\mathbf{q}) = \bar{F}^{I,I'}(-q)$ For the example of quantum Hall ferromagnetism discussed in this paper, $n_A = 0$ and $n_B = 1$ when the bias po-

tential is strong enough to yield complete layer polarization. (The analysis in this section does not apply when both orbital and layer degrees of freedom are in play.) When the A and B orbitals have opposite spins, a common occurrence in quantum Hall ferromagnetism, $F^{A,B}(\mathbf{q}) \equiv 0$. Examples in which the A and B orbitals are centered in different two-dimensional layers require a slight generalization of the present discussion which we do not explicitly address.

Using Eq. (C5) we find (leaving the wave vector dependence of the single-particle and interaction form factors implicit) that

$$
\begin{aligned}
4f^{0,0} &= |F^{A,A}|^2 + |F^{B,B}|^2 + |F^{A,B}|^2 + |F^{B,A}|^2, \\
4f^{0,x} &= 2\ \mathrm{Re}[\bar{F}^{A,A}F^{A,B} + \bar{F}^{B,A}F^{B,B}], \\
4f^{0,y} &= -2\ \mathrm{Im}[\bar{F}^{A,A}F^{A,B} + \bar{F}^{B,A}F^{B,B}], \\
4f^{0,z} &= |F^{A,A}|^2 - |F^{B,B}|^2 - |F^{A,B}|^2 + |F^{B,A}|^2, \\
4f^{x,x} &= 2\ \mathrm{Re}[F^{A,A}\bar{F}^{B,B} + F^{B,A}\bar{F}^{A,B}], \\
4f^{y,y} &= 2\ \mathrm{Re}[F^{A,A}\bar{F}^{B,B} - F^{B,A}\bar{F}^{A,B}], \\
4f^{z,z} &= |F^{A,A}|^2 + |F^{B,B}|^2 - |F^{A,B}|^2 - |F^{B,A}|^2, \\
4f^{x,y} &= 2\ \mathrm{Im}[F^{A,A}\bar{F}^{B,B} + F^{B,A}\bar{F}^{A,B}], \\
4f^{x,z} &= 2\ \mathrm{Re}[F^{A,A}\bar{F}^{B,A} - \bar{F}^{B,B}F^{A,B}], \\
4f^{y,z} &= -2\ \mathrm{Im}[F^{A,A}\bar{F}^{B,A} - \bar{F}^{B,B}F^{A,B}].
\end{aligned}
\tag{C6}
$$

These results are obtained after replacing the pseudospinors by pseudospin direction cosines using

$$
\begin{aligned}
2\bar{z}^A z^A &= 1 + n^z, \\
2\bar{z}^B z^B &= 1 - n^z, \\
2\bar{z}^A z^B &= n^x + in^y.
\end{aligned}
\tag{C7}
$$

Note that because the exchange energy is real, all the interaction form factors are real. The diagonal interaction form factors are even functions of $\mathbf{q}$, while the off-diagonal form factors have both even and odd contributions. The interaction form factors capture the influence of the shape of the pseudospin state dependent cyclotron orbits on exchange energies. In the limit $\mathbf{q} \to 0$, orthogonality implies that $F^{A,B} \to \delta_{A,B}$. If follows that $f^{\alpha,\beta}(\mathbf{q}=0) = \delta_{\alpha,\beta}/2$.

The exchange energy expression can be written in an alternate form by Fourier transforming along the direction perpendicular to the guiding center orbitals, defining

$$
n_p^\alpha = \frac{1}{N_\varphi} \sum_X \exp(-ipX) n_X^\alpha, \tag{C8}
$$

where $N_\phi = 2\pi\ell^2/A$ is the number of guiding center orbitals in a Landau level. The exchange energy then takes a form from which spin-wave dispersions can be simply read off:

$$
E_x = -\frac{1}{2} \sum_p \bar{n}_p^\alpha J_p^{\alpha,\beta} n_p^\beta \tag{C9}
$$

with the momentum space exchange integral given by

$$
J_p^{\alpha,\beta} = \int \frac{d^2\mathbf{q}}{(2\pi)^2} \exp(-ipq_y\ell^2) \exp(-q^2\ell^2/2) f^{\alpha,\beta}(\mathbf{q}) V(\mathbf{q}). \tag{C10}
$$

Because $f^{\alpha,\beta}$ is real, $J_{-p}^{\alpha,\beta} = \bar{J}_p^{\alpha,\beta}$. Similarly, for the diagonal elements of J, the property that the diagonal elements of f are even functions of $\mathbf{q}$ implies that $J_p^{\alpha,\beta} = J_{-p}^{\alpha,\beta}$. Combining both properties, we conclude that the diagonal momentum space interactions are real. The off-diagonal elements, however, can have both even real and odd imaginary contributions. For $p\ell \gg 1$, the integration over $\mathbf{q}$ in Eq. (C10) has contributions from small $\mathbf{q}$ only, allowing us to set $\exp(-q^2\ell^2/2) f^{\alpha,\beta}(\mathbf{q}) \to \delta_{\alpha,\beta}/2$. The integral can then be recognized as an inverse Fourier transform of the electron-electron interaction from momentum space back to real space. It follows that,

$$
J_{p\to\infty}^{\alpha,\beta} = \frac{\delta_{\alpha,\beta} e^2}{2\epsilon|p|\ell^2}. \tag{C11}
$$

This is the familiar peculiarity of quantum Hall systems in which exchange interactions at large momenta are most simply understood[18] after a particle hole transformation which converts them into Hartree interactions between electrons and holes. In strong fields the particle and hole in a magnetoexciton with momentum p are separated in real space by $p\ell^2$. For very large p, the separation between particle and hole is larger than the cyclotron orbit sizes and the interaction is approximately given by the interaction between point charges. For smaller values of p the size and shape of the cyclotron orbit, represented in momentum space by $\exp(-q^2\ell^2/2) f^{\alpha,\beta}(\mathbf{q})$ becomes important.

Imaginary off-diagonal contributions to $J_p^{\alpha,\beta}$ are responsible for DM-like interactions in quantum Hall ferromagnets. In the example discussed in this paper for instance, the A orbital has orbital Landau level index $n=0$, while the B orbital has the same spin and $n=1$. It follows that $F^{A,A} = L_0(q^2\ell^2/2)$ and $F^{B,B} = L_1(q^2\ell^2/2)$, where L_n is a Laguerre polynomial, and that $F^{B,A} = iq\ell\ \exp(i\theta_\mathbf{q})/\sqrt{2}$ where $\theta_\mathbf{q}$ is the orientation angle of $\mathbf{q}$. It follows that $f^{x,y}$ vanishes. The generalized random-phase-approximation that we use in the main text for collective mode calculations is equivalent to linearized pseudospin-wave theory. For fluctuations around a ground state with pseudospin orientation polar angle θ_B (as discussed in the main text), the $J_p^{x,z}$ and $J_p^{y,z}$ pseudospin interactions give rise to DM-like interactions whose strength is proportional to $\sin(\theta_B)$. The DM interactions can be viewed in particle-hole language as a consequence of the property that the interaction between an electron with pseudospin in the $\hat{x}-\hat{y}$ plane at X and a hole with pseudospin in the $\hat{z}$ direction at X' is not invariant under the interchange of X and

X'. This property reflects the pseudospin dependence of dipole and other higher order multipoles in the cyclotron orbit cloud of an electron with a particular pseudospin.

The analysis presented in this section, can be applied to any quantum Hall ferromagnet. One elementary example is the case where the pseudospin orbitals share Landau level index n and have opposite spins. In this case

$$f^{\alpha,\beta} \to \frac{\delta_{\alpha,\beta}[L_n(q^2\ell^2/2)]}{2}. \tag{C12}$$

The pseudospin model has isotropic Heisenberg interactions and the pseudospin-wave excitation energy expression $\omega_p = 2(J_{p=0} - J_p)$, follows immediately from an expansion of the exchange energy function to quadratic order.

[1] H. A. Fertig, Phys. Rev. B **40**, 1087 (1989); A. H. MacDonald, P. M. Platzman, and G. S. Boebinger, Phys. Rev. Lett. **65**, 775 (1990); R. Côté, L. Brey, and A. H. MacDonald, Phys. Rev. B **46**, 10239 (1992); Xiao-Gang Wen and A. Zee, Phys. Rev. Lett. **69**, 1811 (1992); K. Moon, H. Mori, K. Yang, S. M. Girvin, A. H. MacDonald, L. Zheng, D. Yoshioka, and S. C. Zhang, Phys. Rev. B **51**, 5138 (1995); J. P. Eisenstein and A. H. MacDonald, Nature (London) **432**, 691 (2004).

[2] L. Brey and H. A. Fertig, Phys. Rev. B **62**, 10268 (2000); R. Côté and H. A. Fertig, *ibid.* **65**, 085321 (2002).

[3] A. K. Geim and K. S. Novoselov, Nature Mater. **6**, 183 (2007); A. K. Geim, Science **324**, 1530 (2009).

[4] K. S. Novoselov, E. McCann, S. V. Morozov, V. I. Fal'ko, M. I. Katsnelson, U. Zeitler, D. Jiang, F. Schedin, and A. K. Geim, Nat. Phys. **2**, 177 (2006).

[5] E. McCann and V. I. Fal'ko, Phys. Rev. Lett. **96**, 086805 (2006).

[6] M. Koshino and T. Ando, Phys. Rev. B **73**, 245403 (2006).

[7] Yafis Barlas, R. Côté, K. Nomura, and A. H. MacDonald, Phys. Rev. Lett. **101**, 097601 (2008).

[8] K. Nomura and A. H. MacDonald, Phys. Rev. Lett. **96**, 256602 (2006).

[9] Benjamin E. Feldman, Jens Martin, and Amir Yacoby, Nat. Phys. **5**, 889 (2009); Y. Zhao, P. Cadden-Zimansky, Z. Jiang, and P. Kim, Phys. Rev. Lett. **104**, 066801 (2010).

[10] For a commentary and references to related work see K. Novoselov, Nat. Phys. **5**, 862 (2009).

[11] Yafis Barlas, R. Côté, J. Lambert, and A. H. MacDonald, Phys. Rev. Lett. **104**, 096802 (2010).

[12] K. Shizuya, Phys. Rev. B **79**, 165402 (2009).

[13] Cyclotron resonance in bilayer graphene is discussed in D. S. L. Abergel and V. I. Fal'ko, Phys. Rev. B **75**, 155430 (2007); and D. S. L. Abergel and T. Chakraborty, Phys. Rev. Lett. **102**, 056807 (2009).

[14] W. Kohn, Phys. Rev. **123**, 1242 (1961).

[15] I. Dzyaloshinsky, J. Phys. Chem. Solids **4**, 241 (1958); T. Moriya, Phys. Rev. **120**, 91 (1960).

[16] A. H. Castro Neto, F. Guinea, N. M. R. Peres, K. S. Novoselov, and A. K. Geim, Rev. Mod. Phys. **81**, 109 (2009).

[17] I. B. Spielman, J. P. Eisenstein, L. N. Pfeiffer, and K. W. West, Phys. Rev. Lett. **87**, 036803 (2001).

[18] C. Kallin and B. I. Halperin, Phys. Rev. B **30**, 5655 (1984).

[19] J. Nilsson, A. H. Castro Neto, F. Guinea, and N. M. R. Peres, Phys. Rev. B **78**, 045405 (2008).

[20] Eduardo V. Castro, K. S. Novoselov, S. V. Morozov, N. M. R. Peres, J. M. B. Lopes dos Santos, JohanNilsson, F. Guinea, A. K. Geim and A. H. Castro Neto, J. Phys.: Condens. Matter **22**, 175503 (2010).

[21] J. Lambert, R. Côté, Y. Barlas, and A. H. MacDonald (unpublished).

[22] The value quoted by Partoens and Peeters (Ref. 23) is actually $\gamma_4 = -0.12$. But, the parameters of their tight-binding model are defined in a different way from ours and we need to set $\gamma_4 = +0.12$ to reproduce correctly the bilayer energy bands in their Figs. 3 and 4. In Ref. 23, the tight-binding parameters are obtained by comparing the tight-binding model for bilayer graphene with the Slonczewski-Weiss-McClure tight-binding model for bulk graphite (Ref. 24).

[23] B. Partoens and F. M. Peeters, Phys. Rev. B **74**, 075404 (2006).

[24] J. C. Slonczewski and P. R. Weiss, Phys. Rev. **109**, 272 (1958); J. W. McClure, *ibid.* **108**, 612 (1957).

[25] See, for example: A. H. MacDonald, in *Proceedings of the 1994 Les Houches Summer School on Mesoscopic Quantum Physics*, edited by E. Akkermans *et al.* (Elsevier Science, Amsterdam, 1995), pp. 659–720.

[26] The bias must be sufficiently small, however, for the two-band model to be valid. For $\Delta \approx 100$ meV, the kinetic energy of the $N=0$ states are equal to that of the $N=1$ state and Landau level mixing must be considered.